

AD-756 892

INVESTIGATION OF THE SIGNAL ENHANCEMENT
AND DISCRIMINATION CAPABILITIES OF THE
INTERMEDIATE PERIOD STRAIN-PENDULUM
SEISMOGRAPH COMBINATION AT HNME
(HOULTON, MAINE)

Zoltan A. Der

Teledyne Geotech

Prepared for:

Advanced Research Projects Agency

27 September 1972

DISTRIBUTED BY:

NTIS

National Technical Information Service
U. S. DEPARTMENT OF COMMERCE
5285 Port Royal Road, Springfield Va. 22151

**BEST
AVAILABLE COPY**

AD 756892



.....contributing to man's
understanding of the environment world

INVESTIGATION OF THE SIGNAL ENHANCEMENT AND DISCRIMINATION CAPABILITIES OF THE INTERMEDIATE PERIOD STRAIN-PENDULUM SEISMOGRAPH COMBINATION AT HNME (HOULTON, MAINE)

ZOLTAN A. OER
SEISMIC DATA LABORATORY

Reproduced by
NATIONAL TECHNICAL
INFORMATION SERVICE
U.S. Department of Commerce
Springfield, VA 22151

SEPTEMBER 27, 1972

Prepared for
AIR FORCE TECHNICAL APPLICATIONS CENTER
Washington, D.C.

Under
Project VELA UNIFORM

Sponsored by
ADVANCED RESEARCH PROJECTS AGENCY
Nuclear Monitoring Research Office
ARPA Order No. 1714



TELEDYNE GEOTECH
ALEXANDRIA LABORATORIES

90R

DOCUMENT CONTROL DATA - R&D

(Security classification of title, body of abstract and in using annotation must be entered when the overall report is classified)

1 ORIGINATING ACTIVITY (Corporate author)		20 REPORT SECURITY CLASSIFICATION	
Teledyne Geotech Alexandria, Virginia		Unclassified	
		25 GROUP	
3 REPORT TITLE			
INVESTIGATION OF THE SIGNAL ENHANCEMENT AND DISCRIMINATION CAPABILITIES OF THE INTERMEDIATE PERIOD STRAIN - PENDULUM SEISMOGRAPH COMBINATION AT HNME (HOULTON, MAINE)			
4 DESCRIPTIVE NOTES (Type of report and inclusive dates)			
Scientific			
5 AUTHOR(S) (Last name, first name, initial)			
Der, Zoltan A.			
6 REPORT DATE		70 TOTAL NO. OF PAGES	75 NO. OF REFS
27 September 1972		290	20
80 CONTRACT OR GRANT NO.		85 ORIGINATOR'S REPORT NUMBER(S)	
F33657-72-C-0009		294	
9 PROJECT NO.		85 OTHER REPORT NO(S) (Any other numbers that may be assigned to this report)	
VELA T/2706			
ARPA Order No. 1714			
ARPA Program Code No. 2F-10			
16 AVAILABILITY/LIMITATION NOTICES			
APPROVED FOR PUBLIC RELEASE; DISTRIBUTION UNLIMITED.			
11 SUPPLEMENTARY NOTES		12 SPONSORING MILITARY ACTIVITY	
Details of illustrations in this document may be better studied on microfiche.		Advanced Research Projects Agency, Nuclear Monitoring Research Office Washington, D.C.	
13 ABSTRACT			
<p>The intermediate period strain-pendulum combination at HNME is very effective in reducing 1-2 second microtremors and enhancing body phases. The spectra and the relative variation of intermediate period P and S waves show good potential as discriminants between earthquakes and explosions. If, however, discrimination can be made using 1 and 20 second information, then standard instruments have a lower threshold.</p> <p>The spectral behavior of body and surface waves is sensitive to the local structure, and knowledge of the local structure is needed for the refinement of signal processing methods for strain-pendulum combinations. If such knowledge is not available the best method is to design a processor on the basis of noise characteristics alone. Restricting the processor filter to be one-sided relative to zero lag time (physically realizable) degrades the filter performance relative to the two-sided filters but not significantly.</p>			
14 KEY WORDS			
Seismic Strain Signal Processing		Seismic Discrimination P Wave Spectra	

INVESTIGATION OF THE SIGNAL ENHANCEMENT AND DISCRIMINATION
CAPABILITIES OF THE INTERMEDIATE PERIOD STRAIN - PENDULUM
SEISMOGRAPH COMBINATION AT HNME (HOULTON, MAINE)

SEISMIC DATA LABORATORY REPORT NO. 294

AFTAC Project No.:	VELA T/2706
Project Title:	Seismic Data Laboratory
ARPA Order No.:	1714
ARPA Program Code No.:	2F-10
Name of Contractor:	TELEDYNE GEOTECH
Contract No.:	F33657-72-C-0009
Date of Contract:	01 July 1971
Amount of Contract:	\$ 1,736,000
Contract Expiration Date:	31 October 1972
Project Manager:	Robert R. Blandford (703) 836-3882

P. O. Box 334, Alexandria, Virginia

APPROVED FOR PUBLIC RELEASE; DISTRIBUTION UNLIMITED.

TABLE OF CONTENTS

	Page No.
ABSTRACT	
INTRODUCTION	1
INSTRUMENTATION	3
SIGNAL MODELS	5
DATA PROCESSING	14
Two sided filters designed in the frequency domain	15
Wiener filters	19
Discrimination	21
DEPTH PHASES	28
SUMMARY AND CONCLUSIONS	30
REFERENCES	32

LIST OF FIGURES

Figure Title	Figure No.
Displacements and strains caused by an S wave incident on crustal model A at the angle of incidence $i_0 = 21^\circ$ (amplitude of incident wave $1 \mu\mu$).	1
Displacements and strains caused by an S wave incident on crustal model A at the angle of incidence $i_0 = 31^\circ$.	2
Phase angles between strain and displacement due to S waves incident on crustal model A at angles of incidence 21° , 31° and 41° . Prograde or retrograde elliptical particle motion is indicated by letters P and R.	3
Displacements and strains caused by a P wave incident on crustal model A at an angle of incidence $i_0 = 21^\circ$ (amplitude of incident wave $1 \mu\mu$).	4
Displacements and strains caused by a P wave incident on crustal model A at an angle of incidence $i_0 = 31^\circ$.	5
Phase angles between strain and displacement due to P waves incident on crustal model A at angles of incidence 21° and 31° .	6
Unequal cancellation of various modes.	7
Ellipticity/phase velocity ratios derived from earthquake surface waves and noise transfer functions.	8a
Ellipticity/phase velocity ratios for crustal model A.	8b
Ellipticity/phase velocity ratios for crustal model B.	8c
Ellipticity/phase velocity ratios for crustal model C.	8d

LIST OF FIGURES (Cont'd.)

Figure Title	Figure No.
Ellipticity/phase velocity ratios for crustal model D.	8e
Theoretical and experimental strain/pendulum spectral ratios for an earthquake S phase.	8f
Strain (S), filtered pendulum (\tilde{P}) and error (ϵ) trace power spectra using program INOUT on noise sample 1.	9
Strain (S), filtered pendulum (\tilde{P}) and error (ϵ) trace power spectra using program INOUT on noise sample 2.	10
Strain (S), filtered pendulum (\tilde{P}) and error (ϵ) trace power spectra using program INOUT on noise sample 3.	11
F statistic and confidence limits for the existence of transfer function for noise sample 1.	12
F statistic and confidence limits for the existence of transfer function for noise sample 2.	13
F statistic and confidence limits for the existence of transfer function for noise sample 3.	14
Pendulum to strain noise transfer functions for noise sample 1 using program INOUT.	15
Pendulum to strain noise transfer functions for noise sample 2 using program INOUT.	16
Pendulum to strain noise transfer functions for noise sample 3 using program INOUT.	17

LIST OF FIGURES (Cont'd.)

Figure Title	Figure No.
Traces processed by program INOUT. Amplitude is relative.	18
Strain (S), filtered pendulum (\tilde{P}) and error (ϵ) trace power spectra for one sided 64 pt Wiener filter on noise sample 1.	19
Strain (S), filtered pendulum (\tilde{P}) and error (ϵ) trace power spectra for one sided 64 pt Wiener filter on noise sample 2.	20
Strain (S), filtered pendulum (\tilde{P}) and error (ϵ) trace power spectra for one sided 64 pt Wiener filter on noise sample 3.	21
Response of 64 pt Wiener filters designed for noise sample 1 pendulum trace.	22
Response of 64 pt Wiener filters designed for noise sample 2 pendulum trace.	23
Response of 64 pt Wiener filters designed for noise sample 3 pendulum trace.	24
Strain (S), filtered pendulum (\tilde{P}) and error trace power spectra for noise sample 1, after processing by a 64 pt one-sided Wiener filter.	25
Strain (S), filtered pendulum (\tilde{P}) and error trace power spectra for noise sample 2, after processing by a 64 pt one-sided Wiener filter.	26
Strain (S), filtered pendulum (\tilde{P}) and error trace power spectra for noise sample 3, after processing by a 64 pt one-sided Wiener filter.	27

LIST OF FIGURES (Cont'd.)

Figure Title	Figure No.
Response of 64 pt two-sided Wiener filter designed for noise sample 1 pendulum trace.	28
Response of 64 pt two-sided Wiener filter designed for noise sample 2 pendulum trace.	29
Response of 64 pt two-sided Wiener filter designed for noise sample 3 pendulum trace.	30
Events processed by a one-sided 64 pt Wiener filter. Amplitudes are relative.	31
Filtered sum traces for the nuclear explosion TIJERAS. Amplitudes are relative.	32
Filtered sum traces for nuclear explosion CARPETBAG. Amplitudes are relative.	33
Filtered sum traces for a NOVAYA ZEMLYA event. Amplitudes are relative.	34
Filtered sum traces for an earthquake from Guerrero, Mexico. Amplitudes are relative.	35
Filtered sum traces for an earthquake off the coast of Oregon. Amplitudes are relative.	36
Filtered sum traces for an earthquake from Columbia. Amplitudes are relative.	37
Filtered sum traces for an earthquake from North Atlantic. Amplitudes are relative.	38

LIST OF FIGURES (Cont'd.)

Figure Title	Figure No.
Filtered sum traces for an earthquake from Greenland Sea. Amplitudes are relative.	39
Filtered sum traces for an earthquake from Chiapas, Mexico. Amplitudes are relative.	40
Comparison of depth phases on the filtered intermediate period strain-pendulum sum traces with standard LP and SPZ traces. Amplitudes are relative.	41

LIST OF TABLES

Table Title	Table No.
Crustal Models	I
Events Used to Determine E/C Ratios	II

III

INTRODUCTION

It has been recognized for some time that combinations of the strain and pendulum instrument outputs can be used to suppress noise (surface waves) and enhance teleseismic body waves (Romney 1964). The basis for this enhancement is that the spectral amplitudes and phases of various wave types on the two instruments differ. The design of an optimum processor for the strain pendulum combination requires a precise knowledge of the spectral behavior of both the signals and noise. In practice such knowledge is not easily attainable. The spectral behavior of the signal and noise components is a complicated function of the local structure, and this structure must be known in order to determine an accurate signal model. If the local structure is not well known, one often has to use oversimplified signal and noise models.

A considerable amount of work has been done on signal-to-noise ratio enhancement at various locations (Shopland and Kirklin, 1969, 1970, Woolson, 1971). It was found that at some sites, such as WMO, no appreciable noise reduction was attainable, while at other locations (HNME for example) the noise reduction was considerable. At HNME the greatest noise reduction was obtained in the period range 2 - 10 seconds, the range of ordinary "storm microseisms". At shorter periods the coherence between the pendulum and strain instruments falls off due to the increasing complexity of the noise. At longer periods the instrument noise on

both instruments increases, which makes effective noise cancellation impossible.

It has been shown by Shopland (1971) that detection of signals with $T \approx 1$ or 20 seconds at HNME is not significantly aided by combining the strain and pendulum outputs. The reason for this is that the original signal-to-noise ratio is the greatest at periods outside the band of effective noise cancellation. Nevertheless, the enhanced signal exhibits many features which cannot be seen on the standard short and long-period instruments. The 2 - 10 seconds period range, which is dominated by strong microseismic noise, has not been applied extensively to discrimination in the past, and is not covered well by standard instrumentation. It is worthwhile, therefore, to investigate the discrimination capabilities of strain-pendulum combinations in this period range making use of the noise reduction obtainable. This report shows some preliminary results.

INSTRUMENTATION

Details of the instrumentation at HNME have been described by Shopland and Kirklin (1970). Both strain and pendulum instruments operate with velocity transducers; with the exception of a low pass filter which operates on the strain output only, the signals pass through identical amplifiers and filters to the tape recorder. The low pass filter has a 6 dB/octave-slope over the signal frequency range to enhance the strain output at long periods, since the displacement differential between the two ends of the strainrod rapidly decreases with period (and wavelength) for both noise and earthquake signals. This filter therefore approximately equalizes the background noise spectra on the two instruments and shifts the relative phase on the two recording channels to 90° for Rayleigh waves (the true strain-to-displacement ratio phase shift is 0 or π for surface waves). If the low-pass filter is removed, the recording system is matched; that is, for the same strain-to-displacement ratio, the output spectra are proportional. The processing filters used in this report for noise equalization shift the phase to correct for the 90° phase shift of the band-pass filter and adjust the amplitude response of the processor for any slight deviations of the strain-to-displacement ratios on the two data traces. After the amplitudes and phases of the noise on the two traces are equalized, the noise is reduced by taking the difference of the equalized traces. The above information is necessary for the understanding of the rest of this report, since the

theoretical calculations we present show the true amplitude - phase relations between vertical displacement and strain, while the data analysis uses the pre-filtered strain data.

SIGNAL MODELS

All seismic waves originating from a distant event are of some interest and can be defined as signals. In detection and discrimination work it is desirable to enhance all waves of interest and reduce local ambient noise. While the ambient noise is slowly changing and can be considered relatively stationary in time, the signals of interest consist of short transients such as various compressional and shear wave phases with different angles of incidence, and the surface wave signals. The various wave types interact with the local structure in different ways and produce waveforms with characteristic phase and amplitude relationships on the two instruments. These differences in behavior are used to distinguish various phases, but also complicate the task of designing an optimum processor for strain-pendulum combinations.

Since most of the background noise which can be cancelled by equalization consists of surface waves, the processors will tend to cancel the surface wave part of the signals also. At the same time the body waves which have quite different relative phase characteristics will be enhanced or reduced at a lesser degree. Therefore, the signal model for the body waves will be discussed first.

A simple signal model can be constructed for incident P and S waves by assuming that the local structure can be modeled by a homogeneous elastic half-space (Woolson, 1970). This model predicts that

incident P waves are predominant on the vertical pendulum outputs, while S waves usually appear on the strain instrument outputs with the largest amplitude for angles of incidence which are common for teleseisms. If the local surface phase velocity of S waves falls below the compressional velocity in the half-space, the vertical motion becomes elliptical and behaves similarly to a surface wave. This occurs only for relatively near earthquakes.

Although the half-space model roughly predicts the behavior of body waves, it is a gross approximation. It has been shown that for harmonic unidirectional waves the vertical strain at the surface is related to the horizontal displacement by the general relationship

$$\frac{\partial w}{\partial z} = -i \left(\frac{\omega}{c} \right) \left(\frac{2\beta^2}{\alpha} - 1 \right) u$$

where u is the horizontal displacement, ω is the angular frequency, c is the phase velocity, α is the compressional and β is the shear velocity at the surface. For surface waves the horizontal displacement can be expressed as

$$u = iEw$$

where E is the ellipticity of vertical motion. E is a

function of the local structure and the mode considered. For body waves incident on a layered medium the horizontal displacement is a complicated function of the period and the angle of incidence (Haskell, 1962).

In order to see the magnitude of the difference between the half-space model and the crustal structure some calculations were made for a crustal model A shown in Table I. The actual crustal structure in the immediate vicinity of HNME (Houlton, Maine) is not known but this model represents an average "crust" which is not an unreasonable assumption for the regional structure. Figures 1 through 3 show the results for S waves incident with an amplitude of 1.0μ . Figures 1 and 2 show the strain and displacement at two angles of incidence (measured from the vertical) for S waves. Solid straight lines on Figure 1 show the slopes of the corresponding results for a halfspace. The figures show that the spectral amplitudes at certain periods can differ considerably from those predicted by the half-space model even if one disregards some narrow notches in the spectra which have little influence on the overall spectral behavior. Discrepancies between the two models in amplitude amount to ratios of 0.5 - 2 over broad frequency ranges. In Figure 3 which shows the phase angles, it can be seen that while the phase difference oscillates around 90° , the value appropriate to the half-space model, it is smaller in value and at places it differs from 90° by as much as 70° . At the top of the figure the phase angles for the angle of incidence $i = 41^\circ$ are shown. At this angle the surface phase

TABLE I
Crustal Models

MODEL A

d	α	β	ρ
5.	4.	2.3	2.6
32.	6.285	4.635	2.869
∞	7.96	4.6	3.37

MODEL B
(Thicker Crust)

d	α	β	ρ
5.	4.	2.3	2.6
42.	6.285	4.635	2.869
∞	7.96	4.6	3.37

MODEL C
(Thicker Sediments)

d	α	β	ρ
10.	4.0	2.3	2.6
27.	6.285	3.635	2.869
∞	7.96	4.60	3.37

MODEL D
(Thinner Sediments)

d	α	β	ρ
2.	4.	2.3	2.6
35.	6.285	3.635	2.869
∞	7.960	4.600	3.370

velocity falls below the compressional velocity in the half-space. The phases for this angle of incidence are similar to those of the surface waves but alternating between prograde (Pr) and retrograde (Rr) motion, the surface motion at this phase velocity is essentially dominated by coupled leaky modes (Su and Dorman 1965). The exact 0° and 180° values for phase-shift are naturally not realistic since these values are the results of the arbitrary termination of the model with a half-space below the Mohorovicic discontinuity. Addition of some mantle layers would change the results somewhat, but probably not essentially since the velocity transitions in the upper part of the mantle are presumably more gradual and attenuation would tend to eliminate sharp resonances. When cancelling surface wave noise by equalizing the noise phases and spectra, the retrograde portions of S waves will tend to be reduced and the prograde portions to be enhanced.

Figures 4 to 6 show similar graphs for incident P waves. The figures show the preponderance of P waves on the displacement sensors (pendulum) relative to the strain instrument and reveals essential differences between the half-space and layered models as did the S waves.

The surface wave portion of the signal will have a tendency to behave like the noise and will be attenuated by the processors, but not in the same degree as noise since the surface wave signals generally differ in spectra and modal composition from noise background. Fundamental mode Rayleigh wave signals contain

longer periods, and the higher modes in signals are concentrated mostly in the main microseism period band whereas the background noise consists of fundamental mode Rayleigh waves at most sites. Since the processor is designed to cancel fundamental mode surface waves, higher modes will not be as effectively attenuated. This is due to their different particle motion ellipticity to phase velocity ratios (E/C) (Oliver, Dorman, and Sutton, 1959; Oliver and Ewing, 1957). For some structures the higher mode surface waves possess a prograde particle motion for certain period ranges. The processor would enhance these waves. Figure 7, for instance, shows the playback of an event from the Gulf of California as processed by the on-line analog system at HNME. The sum of the analog phase-shifted strain and pendulum instruments shows a train of short-period waves of high group velocity. These are higher surface wave modes which are imperfectly cancelled by the on-line processor. The longer period surface waves which follow these are attenuated more strongly. The sum trace in the figure is not on the same scale as the strain and pendulum traces; this is of no consequence, however, in demonstrating the relative difference in the cancellation of various modes.

Summing up the above results, the body wave signal properties for realistic earth models are sufficiently different from those of the surface wave noise that it is possible to reduce the noise considerably using a suitable processor without significantly degrading the signals. This is, however, not true for all frequencies

and angles of incidence. This is the reason why it is desirable to obtain some knowledge of the local structure in order to predict the signal characteristics and refine the processors.

The simplest approach is to model the local structure with a set of horizontal homogeneous elastic layers. Spectral ratios of various wave types can then be used to determine a model which fits these spectral ratios. If body waves are used, this approach is essentially identical to that of Phinney (1964), except for a multiplicative factor

$$i\left(\frac{\omega}{c}\right) \left(\frac{2\beta^2}{\alpha^2} - 1\right)$$

which distinguishes the strain from the horizontal displacement. The method can also be used with surface waves, as was done by Boore and Toksöz (1969). Naturally, if the local structure is laterally inhomogeneous it may not be possible to fit the data by any model.

Some attempts were made to fit the observed ellipticity to phase velocity, and body wave spectral ratios to a horizontally layered local structure at HNME. This task was not completed since the available set of data was not suitable to derive the local structure with any certainty. The main difficulties were caused by the inadequate calibration at HNME and the unavailability of events with high signal-to-noise ratio for the body phases. It soon became obvious that

the surface wave ellipticity to phase velocity ratios as derived from the data cannot be explained by any reasonable earth structure. This was attributed to an error in the strain calibrator. This error was assumed to be frequency independent, causing all ratios to be in error by the same factor. The second source of difficulty was the high operating gain at the site which resulted in the clipping of all large events with high S/N ratio on the tape recordings. This difficulty could have been easily avoided if low-gain traces had been recorded instead of the phase-shifted pendulum and strain outputs which are completely redundant. During the operation of the system several large events occurred which could have been saved for analysis in this way.

Figure 8a shows the ellipticity/phase velocity ratios (E/C) derived from Rayleigh waves from various earthquakes. The earthquakes used are described in Table II. The ratios were measured by hand from film and reduced to the same relative scale. Besides the fundamental mode observations there is an observation for first higher mode, which is marked by a star on the figure. The ratios seem to have a peak around 12 seconds period for the fundamental mode. The particle motion for all observations is retrograde. The rise of the curve towards the shorter periods is based on the noise pendulum-to-strain transfer functions which, as shown later, rise towards the short period end of the spectra, indicating a rising E/C ratio for background noise. It is known from the literature that the micro-seismic background consists of fundamental mode waves

TABLE II

Events Used to Determine E/C Ratios

1) December 1, 1970 51.4N 175.3W	t = 21 ^h 09 ^m 37.2 ^s Andreanoff Islands	m _b = 5.6
2) December 4, 1970 23.1S 70.1W	t = 17 ^h 08 ^m 48.7 ^s Near coast of Northern Chile	m _b = 5.9
3) November 18, 1970 35.1N 35.7W	t = 12 ^h 23 ^m 18.0 ^s North Atlantic Ridge	m _b = 5.4
4) November 26, 1970 43.8N 127.4W	t = 03 ^h 11 ^m 42.8 ^s Off the coast of Oregon	m _b = 5.6

around 6 - 8 second period at most places. (Douze 1964, Blake and Donn 1954.) Admixture of higher modes may contribute to the decrease of coherence at shorter periods, especially if their particle motion is prograde, but fundamental mode waves seem to dominate, since the E/C ratios would decrease with decreasing period if the modal composition changed substantially.

Figures 8b through 8e show curves of E/C vs period for various structures. The parameters of these structures are given in Table I. The sensitivity of the ratio to structural changes is quite obvious from the figure. None of the given models satisfy the data in Figure 8a exactly, but allowing for a possible scale factor, Model B is the best. Model D changes in the right sense relative to initial Model A, but too much. Therefore it seems that a good fit can be achieved by increasing the crustal thickness and/or decreasing the sediment thickness relative to Model A.

Figure 8f shows spectral amplitude ratios for S waves observed at HNME. The theoretical curve is for Model A. The event used was an earthquake in the North Atlantic (November 18, 1970, 12^h23^m18.0^s, 35.1N, 35.7W, $M_s = 6$). This earthquake occurred at a relatively short distance from HNME and for this reason the amplitudes on the strain and pendulum traces are comparable and the particle motion is elliptical. This was the only body wave in the data where the original S/N ratio was acceptable on both instruments. The observed spectral ratio does not fit the data, and only a vague similarity exists between the observed and the theoretical curve.

It could have been compared to other models to improve the fit but this was not pursued since in the absence of more data, the results could not have been verified. Besides, arrivals from many different azimuths are necessary to rule out lateral inhomogeneity at the site. The above discussion proves, however, that if care is taken to preserve large S/N ratio events, the spectral ratio method is sensitive enough to narrow the range of possible local structural models. Knowledge of the local structure could then be used to establish reliable signal models and refine the processor for the site.

DATA PROCESSING

Three processors were used to process data in this study:

1. Two-sided 128 pt filters designed in the frequency domain.
2. One-sided 64 pt Wiener filters.
3. Symmetrical 64 pt Wiener filters.

The purpose of digital processing is to test whether or not the inherent one-sidedness (physical realizability) of analog filters impairs the noise reduction appreciably, and to exploit the flexibility of digital filters with regard to amplitude and phase characteristics and their adaptability to changing noise conditions.

There can be three different approaches to the elimination of noise on vertical pendulum and strain combinations. The maximum likelihood approach requires that the signal waveform (defined in some manner) is constrained to remain undistorted while the noise is optimally reduced. This constraint presupposes a knowledge of the amplitude and phase relationships of the signal and the spectral characteristics of the noise on both instruments. If the constraint of absence of signal distortion is strictly adhered to, a severe limitation in the noise reduction capability of the processor may result.

Another approach may require that the signal is reproduced optimally by reducing the root-mean-square error between the desired output (signal) and the

output of the system. This is the classic Wiener criterion. This approach does not require an exact knowledge of the signal model, but only approximate estimates of the signal correlation functions. Finally, one can design a processor in such a way that the noise is optimally reduced between the two channels without giving any consideration to the effect of the processor on the signal, as long as it is passed in some form. Such a process has been operated on-line at HNME and consisted of analog phase shift networks operating on the two channels and taking the difference of a suitable pair of phase shifted channels.

Since there is little hope that the exact signal strain to pendulum transfer function will be known at any site, and because the background noise in the period range to be investigated (2-8 sec) is so overwhelming, one must use the two approaches last mentioned, favoring the third approach of simple noise cancellation.

If the exact arrival time of the signal is of interest, one must restrict the processor to be physically realizable in order to avoid precursors. This restriction may not be very severe since the analog networks used at the sites performed quite well.

Two sided filters designed in the frequency domain

This processor uses a computer program (INOUT) written by R. Shumway (personal communication, 1971). The computer program designs digital filters from the

equation

$$H(f) = \frac{P_{xy}(f)}{P_{xx}(f)}$$

where $H(f)$ is the transfer function of the filter $P_{xy}(f)$ and $P_{xx}(f)$ are the cross power spectra between the input card desired output and the autopower spectrum of the input respectively. The program computes the power spectra by Fourier transforming the data trace, taking the dot product of Fourier spectra, smoothing the result by running averages and decimating to obtain power spectra. The program applies the filter to the sample and computes the filter amplitude and phase characteristics, the power spectra of the raw input, and filtered (equalized) difference (error) traces. It also gives a table of the power ratio of the equalized and error traces. This quantity possesses a non-central F distribution and confidence limits can be set to test the degree of inter-dependence of the traces as a function of frequency. Figures 9 through 11 show the results of the application of this program to three noise samples, given in Table II. In the figures P is the power spectrum of the filtered pendulum trace, S is the strain power spectrum and ϵ is the power spectrum of the difference (error) trace. The figures show that the noise spectrum and the degree of cancellation change appreciably from time to time. Sample 1 shows the noise cancellation which is the least effective, while Sample 2 shows a very effective cancellation reducing

the noise power by a factor of 20 at the peak. At the long periods, above 10 seconds period, the power spectrum of the strain is considerably higher than that of the equalized pendulum. This is interpreted as uncorrelated system noise on both instruments, which indicates that the data cannot be trusted above 10 second period.

The above spectra were computed using 1024 point noise samples sampled at 2.5 samples/sec from which power spectra were computed resulting in 64 spectral points after smoothing and decimating. Figures 12 through 14 show plots of the corresponding F statistics. The 90 percent and 95 percent confidence limits for the existence of transfer functions between the two time series are indicated. The figures show that the most coherent range is between 2-7 seconds period for the strain and pendulum instruments. Low values of the F statistic above 10 second period indicate that the noise is uncorrelated on the two instruments.

Figures 15 through 17 show the amplitude and phase responses of the resulting filters. At long periods ($T > 10$ sec) the filters behave quite erratically, and between the periods of 8 to 2 seconds the amplitude response rises towards shorter periods. They exhibit erratic behavior also at the short period end. The relative phase shift of the filters is fairly constant between 1.5 - 10 seconds period, in a range somewhat wider than the range of substantial coherence. This is in agreement with the notion that the noise in the short period end consists of a mixture of various Rayleigh

wave modes with the same relative phase but different relative amplitudes. The phase is essentially zero at about 1 second period indicating the predominance of in-phase system noise on both instruments.

Figure 18 shows some processed seismograms of several events. The traces from top to bottom are the pendulum, strain, the filtered pendulum and the difference trace. Comparison of the original and difference traces reveals a significant reduction of noise with the result that phases which are weak on the original traces can be seen more clearly on the difference trace. This is evident for S phases which cannot be recognized with certainty on the original traces. The surface wave trains were not reduced much by the processor. This is caused by the absence of coherent noise energy at long periods which characterize the surface wave train. The equalizing filter which was computed from the noise sample will thus reduce the long period content of the filtered pendulum trace. When the difference is taken the surface wave portion is not equalized and retains its high amplitudes. The phases on the difference trace also exhibit many characteristic individual details which usually cannot be seen on the standard short-period and long period instruments. Because of the two-sidedness of the filter used, all major phases show some precursors. This is undesirable if an accurate determination of arrival times is needed. The application of one sided (physically realizable) filters can eliminate this problem, but at the same time some effectiveness in noise reduction has to be sacrificed.

Wiener filters

Equalization and cancellation of the noise on strain and pendulum instruments can also be achieved with Wiener filters calculated in the time domain from the noise correlation functions using the Levinson recursion method. These filters will be the most effective at the coherent spectral peaks and will also tend to reduce the amplitude of noise at frequencies where the coherence is low. These filters can be easily restricted to be one-sided, while applying the same constraint to filters designed in the frequency domain is considerably more complex.

To derive the Wiener filters, correlation functions were computed by Fourier transforming the noise traces, computing the appropriate dot products, and by transforming back into the time domain. The resulting correlation functions were tapered using a Parzen window the same length as the desired filter. This procedure introduces smoothing of the filter frequency responses and also stabilizes the recursive calculations used to derive the filters.

Figures 19, 20, and 21 show the noise reduction achieved by a 64 point one-sided Wiener filter on the noise sample tested before. At first glance it would seem that the noise reducing capabilities of these filters are considerably worse than those of the filters designed in the frequency domain. Closer inspection reveals, however, that most of the visible differences in the spectra are due to the different smoothing used in the spectral calculations. The spectra

of the Wiener filter calculations are smoothed more.

Figures 22, 23, and 24 show the frequency response of the one-sided Wiener filters. The amplitude responses increase toward the shorter periods.

Figures 25 to 27 show the noise reduction for a two-sided 64 point Wiener filter (with zero lag at the middle). These results are directly comparable to those for the one-sided filter, since the spectral smoothing applied is the same. The comparison shows that, as is to be expected, the two-sided filter reduces the noise more effectively, but the difference is not very great. It does not exceed the power ratio of 1.5 at the main spectral peak, but it may be 2 at the shorter periods, around 2 - 3 seconds. The filter length does not seem to be an important factor since the filter weights rapidly diminish from the beginning of the filter in the one-sided case or towards both ends in the two-sided case. Therefore, it seems that increasing the lengths of filters would not alter the response substantially. The amplitude and phase responses of the one-sided filters show that they essentially differentiate the input. The two largest weights are two nearly equal numbers of opposite sign at one end of the filter. The two-sided Wiener filters are more complex; they have a phase-shift close to 90° and nearly constant amplitude response throughout the coherent period range of the noise with a slight increase towards the shorter periods as shown in Figures 28, 29, and 30. Since the two-sided filters are not limited by the severe constraint of physical realizability, their response functions

are more likely to be characteristic of the dominant ellipticity/phase velocity (E/C) ratio of the noise. The above results indicate the average E/C ratio of background noise slowly increases with the decreasing period in the period range 2 - 10 seconds.

Figure 31 shows the three previously (Figure 18) shown events processed by a one-sided Wiener filter. The precursors are absent and the arrival times are distinct. The noise reduction capability is not inferior to the previous processor, it may be somewhat better. This difference may be attributed to some non-stationarity of the noise, since the processors were designed from noise samples preceding the events by several minutes.

Discrimination

The most successful discrimination criteria, $M_s - m_b$ and various spectral ratios, are based on the differences in the excitation of various wave types and periods between earthquakes and explosions. These differences are due to different source time functions, dimensions, mechanisms and depths for earthquakes as compared to explosions. The ability of strain-pendulum combinations to reduce noise in the main microseism band makes effective application of discriminants for smaller magnitude events possible within this band. In the following, a set of earthquakes and explosions will be shown and the differences in their features will be pointed out. The explosion data set includes only three, fairly large, nuclear explosions from NTS. The available data were limited by the fact that the

extended-period strain-pendulum combination was operational only for about six months. In spite of the incompleteness of the data set, the explosions and earthquakes are strikingly different, and the differences are not likely to be caused entirely by path effects. Originally, digital spectral analysis of the enhanced body waves of strain-pendulum combinations was planned. Due to difficulties with the digital computer the seismograms were processed by analog techniques; the strain-pendulum sum trace was passed through a set of narrow-band analog Krohn-Hite filters and displayed on a chart recorder. The cutoffs of the various bands are the following from the top to the bottom of Figures 32 through 40.

- .05 - 10.0 cps wide band
- .1 - .2 cps low frequency band
- .2 - .5 cps middle band
- .5 - 1.25cps high frequency

Figures 32 through 40 illustrate a set of characteristic events. All events shown have body wave magnitudes over 5, and the epicentral distances to HNME are comparable (with one exception).

Inspection of the figures reveals striking differences between the explosions and earthquakes; some of which may be of use as countermeasures against arrays of large explosions.

In the following we discuss all the events in the set individually. In the first three figures the recordings of three nuclear explosions are shown

(Figures 32, 33, and 34). The first example is the nuclear explosion Tijeras at NTS (Figure 32). It shows a prominent P wave which is concentrated predominantly in the high frequency band. There is a recognizable P wave in the middle band too. The traces for the nuclear explosion Carpetbag show the same thing (Figure 33). The wide band trace shows some long-period noise for this event. The expected arrival times of some other phases are marked for both explosions but none of these are clearly recognizable on the traces shown. Figure 34 shows an event from Novaya Zemlya with a much larger magnitude ($m_b = 6.7$ USC&GS). It shows P arrivals on all four bands, but with the short-period band predominating. There is a clear PcP arrival. Expected arrival times of some other phases are marked but they cannot be recognized on the traces with any certainty.

The recordings of explosions show significant differences when compared to earthquakes. Figure 35 shows an earthquake from Guerrero, Mexico. It has a P phase with the largest amplitude in the middle band; a PP phase is also present. S phases are not clearly indicated on this record. The earthquake off the coast of Oregon (Figure 36) shows a P phase roughly evenly distributed among the three bands, a couple of phases consisting of PP, PPP and possibly PcP, and a clear S on the low frequency and wide bands. The large amplitudes at the end of the traces are probably higher mode Rayleigh waves which were not cancelled by the on-line processor.

The Colombia earthquake (Figure 37) shows again a

wide band P wave, a complete set of arrivals consisting of PP, PPP and PcP, and clear S phases which are not evident in the short period band but are present in other bands. SS is likely to be present also. The depth phase pP is also present in the short period band.

The earthquake in the North Atlantic is at a shorter epicentral distance. It has a large complex P phase (Figure 38) which shows the largest amplitude in the high frequency band. A strong S phase is also present.

The Greenland Sea earthquake shows broad band P phases, some indications of S. (Figure 39).

The earthquake from Chiapas, Mexico (Figure 40) is similar in character; there is some indication of S and SS but very vague. An interesting feature of this earthquake is the pP phase on the middle band trace. Of the many events which were examined, this is the only instance where the pP phase is the clearest in the middle frequency band. The middle and low frequency bands in all the other examples did not enhance the pP phase relative to the conventional short period recordings.

All the explosion events show a prominent P phase with most of the energy concentrated at the short period end of the spectrum and falling off sharply to longer periods. The earthquake P phases, on the other hand, contain relatively more energy at the longer periods. This is another example of the effectiveness of spectral discriminant proposed by Pasechnik (1967)

and also demonstrated by Wyss, Hanks, and Liebermann (1971), and Molnar (1971). Besides the differences in the P spectra there is the total absence of multiple P, (PP, PPP) and S phases on the explosion recordings, while the same phases are quite apparent on the earthquake records. There is no simple explanation for these differences.

The propagation paths for the explosion and earthquake events shown are admittedly different. Two of the explosions originated at NTS in a geophysically peculiar region with high attenuation and other anomalous features (Archambeau, Flinn, and Lambert, 1968; Molnar and Oliver, 1969). The Novaya Zemlya event, however, originates from a stable shield type region with none of the anomalous features associated with the Basin and Range structure. The earthquake signals come from a wide variety of regions. The dissimilarity of paths alone, therefore, does not seem to explain the observed differences in the appearance of the seismograms shown. The absence of the S on NTS explosion recordings could be explained with high attenuation under NTS but this does not explain the absence of S from the event at Novaya Zemlya and S phases for nuclear explosions at NTS which were observed at other sites, although not frequently (Nuttli, 1969; Hirasawa, 1971) for large events but amplitude of S phases from explosions is relatively lower than for earthquakes, and therefore seems to be associated with the source mechanism. The absence of PP phase is even more puzzling. PP readings seemed to be quite common at

other sites at comparable distances from NTS on the short-period instruments. Of about 12 large NTS explosions, only one PP phase was reported at HNME. Whether this was due to the high noise level at HNME on the raw short period pendulum output or to some peculiar path effect is not known.

Summarizing the above observations, the observed differences in the P spectra of earthquakes and explosions seem to be real and due to the source. The differences in the excitation of S phases is probably real also, but attenuation under NTS may considerably enhance this difference. The absence of PP on explosion recordings at HNME is not explained; it is conceivable that since the explosions generate very high frequency P waves these waves get attenuated more by passing repeatedly through the low velocity layer in the upper mantle than ordinary longer period P waves from earthquakes.

It is interesting to speculate what effect the application of the above potential discriminants, intermediate period P spectra, and relative excitation of SV waves, could have in detecting evasive measures such as shot arrays. The ratio of 1 second to 6 second energy is likely to be as diagnostic as 1-second to 20 second energy. However, it should not be so easy to superimpose 6 second energy to simulate an earthquake as it is to superimpose 20 second energy. If the relative excitation of intermediate period SV turns out to be a diagnostic, shot arrays will not be able to confuse this discriminant since the excitation of SV is closely

related to the nature of the source mechanism, which remains a point compressive source, regardless of any space-time configuration.

DEPTH PHASES

Shopland (1971) proposed that further research should be done to determine whether the extended period instruments are useful in identifying depth phases. The difference traces of a large number of events were examined for depth phases. The difference trace was filtered to show four different frequency bands and a wide band trace was also displayed. The traces were compared to the standard short period vertical trace. Figure 41 shows a typical situation encountered for P phases. The standard short period instruments show a well developed pP phase which also can be seen on the shortest period band pass filtered difference trace. The other bands and the wide band difference trace, however, do not show easily recognizable pP phases. This means that including the intermediate band contribution, where the noise cancellation is the most effective, does not improve the detection of the pP phase. In the short period part of the spectra pP is easily recognizable but the noise cancellation procedure is considerably less effective. The situation is somewhat different for S phases. S phase spectra are peaked at longer periods and S phases can only rarely be seen on the short period instruments, while at intermediate periods, 5 - 8 seconds, they are quite common. The data seem to indicate that depth phases such as sS, if present, are better defined in the intermediate period band. The same phases are ill defined on the standard long period instruments. An example of this is shown in the same figure which shows a possible sS phase;

the same phase is not well recognizable on the standard long period vertical instrument and not visible at all in the short period band.

SUMMARY AND CONCLUSIONS

The surface and crustal structure at the recording site modifies the spectral ratios of incident body waves to a considerable degree relative to the simple half-space model.

If the equalizing filters are restricted to be one sided the effectiveness of the filter is degraded by a few dB in amplitude relative to the more general two sided filters.

The E/C ratio of background noise increases slowly with decreasing period at HNME.

The E/C ratio of surface waves shows a peak of 13-14 second period at HNME.

S wave spectral ratios were computed for one earthquake but were not fitted to a theoretical model.

The strain-pendulum combination proved to be useful in increasing the discrimination capabilities of the station at HNME in the intermediate period band by reducing the background noise, but the detection capabilities are poor at the site.

Significant differences between earthquakes and explosions were found in the intermediate period P and S wave spectra. Part of the S wave spectral differences can be explained by greater attenuation under NTS. The absence of PP phases at HNME for explosions is unexplained.

Some discriminants which use intermediate period information are potentially useful in detecting shot arrays.

Strain-pendulum combinations are not useful in enhancing depth phases except possibly intermediate period S depth phases such as sS.

Combination of intermediate period strain and pendulum instruments, in general, are not useful to lower the detection threshold of seismic events at either $T = 1$ or $T = 20$ since the signal to noise ratio is better on the standard short and long period instruments than on the sum traces as can be seen in Figure 41.

REFERENCES

- Archanbeau, C.B., Flinn, E.A., and Lambert, D.G., 1969, Fine structure of the upper mantle; J. Geophys. Res., v. 74, p. 5825-5865.
- Blake, M. and Donn, W.L., 1954, Microseism ground motion at Palisades and Weston; Bull. Seism. Soc. Am., v. 44, p. 597.
- Boore, D.M. and Toksöz, M.N., 1969, Rayleigh wave particle motion and crustal structure; Bull. Seism. Soc. Am., v. 59, p. 331-346.
- Douze, E.T., 1964, Rayleigh waves in short period noise; Bull. Seism. Soc. Am., v. 54, p. 1197-1212.
- Haskell, N., 1962, Crustal reflection of P and SV waves; J. Geophys. Res., v. 67, No. 12, p. 4751-4767.
- Hirasawa, T., 1971, Radiation patterns of S waves from underground nuclear explosions; J. Geophys. Res., v. 76, p. 6440-6454.
- Molnar, P. and Oliver, J., 1969, Lateral variations of attenuation in the upper mantle and discontinuities in the lithosphere; J. Geophys. Res., v. 74, p. 2648-2682.
- Molnar, P., 1971, P wave spectra from underground nuclear explosions; Geophys. J. R. Astr. Soc., v. 23, p. 273-287.
- Nuttli, O.W., 1969, Travel times and amplitudes of S waves from nuclear explosions in Nevada; Bull. Seis. Soc. Am., v. 59, p. 385.

REFERENCES (Cont'd.)

- Oliver, J., Dorman, T. and Sutton, G., 1959, Second shear mode of continental Rayleigh waves; Bull. Seism. Soc. Am., v. 49, p. 379.
- Oliver, J. and Ewing, M., 1957, Higher modes of continental Rayleigh waves, Bull. Seism. Soc. Am., v. 47, p. 187-204.
- Papoulis, A., 1965, Probability, Random variables and stochastic process; McGraw Hill Book Co., New York.
- Phinney, R.A., 1964, Structure of the Earth's crust from spectral behavior of long period body waves; J. Geophys. Res., v. 69, p. 2997-3017.
- Shopland, R.C. and Kirklin, R.H., 1969, Application of strain seismographs to the discrimination of seismic waves; Bull. Seism. Soc. Am., v. 59, p. 657-691.
- Shopland, R.C., 1971, Evaluation of the intermediate period strain system at HNME; Geotech Teledyne, Report No. TR-71-4.
- Shopland, R.C. and Kirklin, 1970, Application of a vertical strain seismograph to the enhancement of P waves; Bull. Seism. Soc. Am., v. 60, p. 105-124.
- SIPRI, 1968, Seismic methods for monitoring underground explosions Intern. Inst. for Peace and Conflict Res. Stockholm.

REFERENCES (Cont'd.)

- Su, S.S. and Dorman, J., 1965, The use of leaking modes in seismogram interpretation and in studies of crust mantle structure; Bull. Seism. Soc. Am., v. 55, p. 989-1021.
- Woolson, J.R., 1970, Analysis of strain seismograph data; Seismic Data Laboratory Report No. 250, Teledyne Geotech, Alexandria, Virginia.
- Wyss, M., Hanks, T.C. and Liebermann, R.C., 1971, Comparison of P wave spectra of underground explosions and earthquakes; J. Geophys. Res., v. 76, p. 2716-2729.

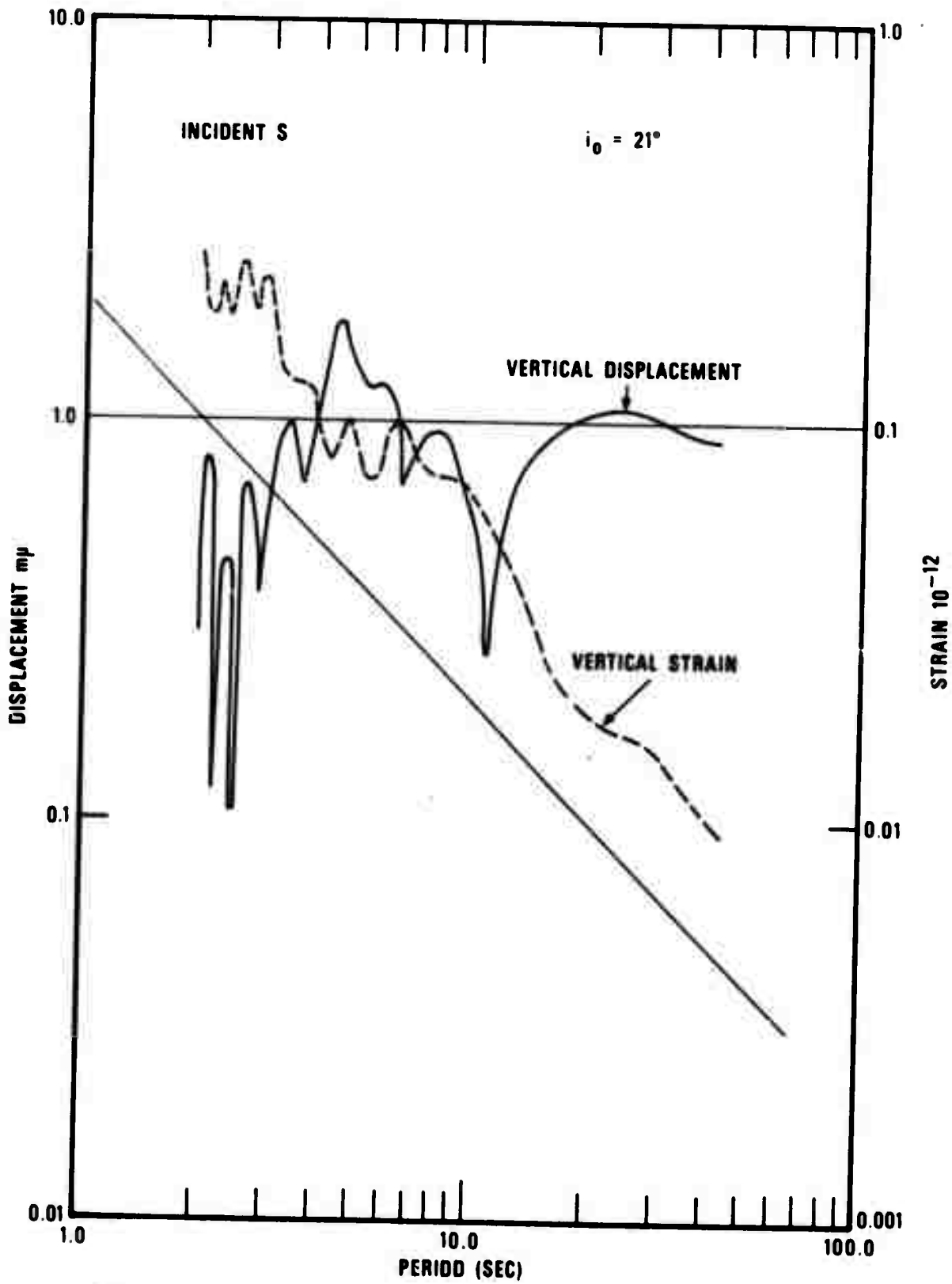


Figure 1. Displacements and strains caused by an S wave incident on crustal model A at the angle of incidence $i_0 = 21^\circ$ (amplitude of incident wave 1 $m\mu$).

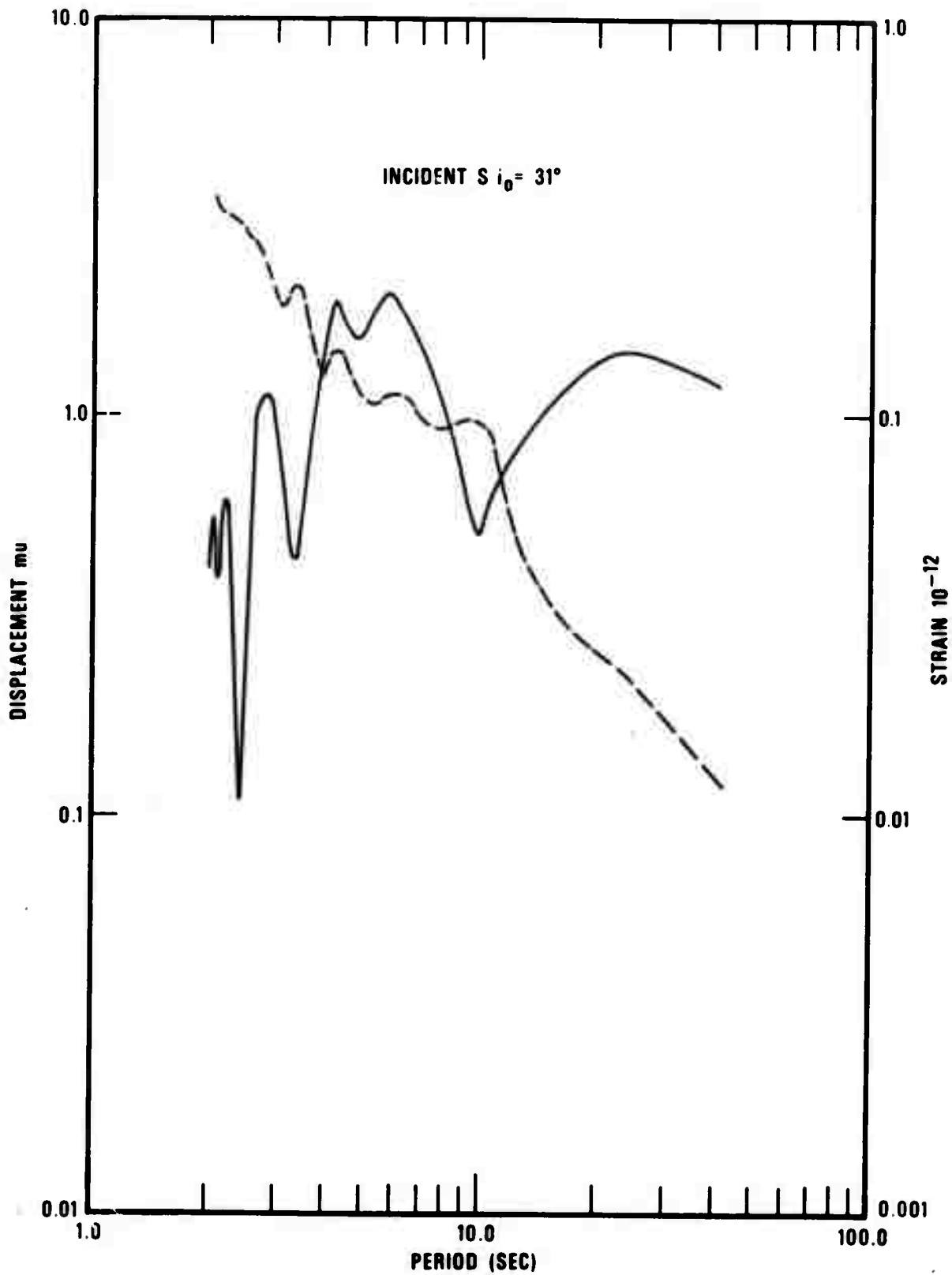


Figure 2. Displacements and strains caused by an S wave incident on crustal model A at the angle of incidence $i_0 = 31^\circ$.

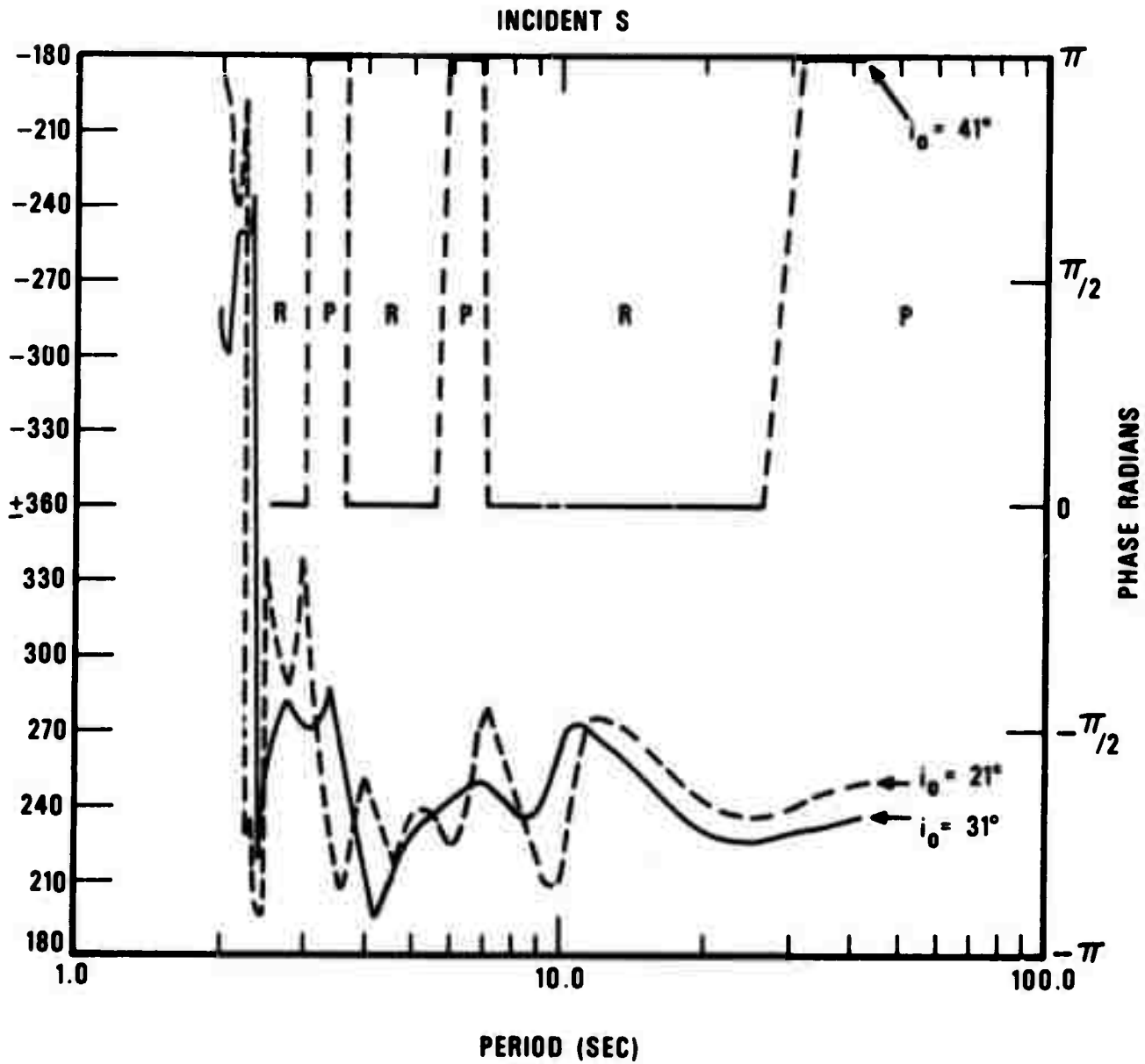


Figure 3. Phase angles between strain and displacement due to S waves incident on crustal model A at angles of incidence 21° , 31° and 41° . Prograde or retrograde elliptical particle motion is indicated by letters P and R.

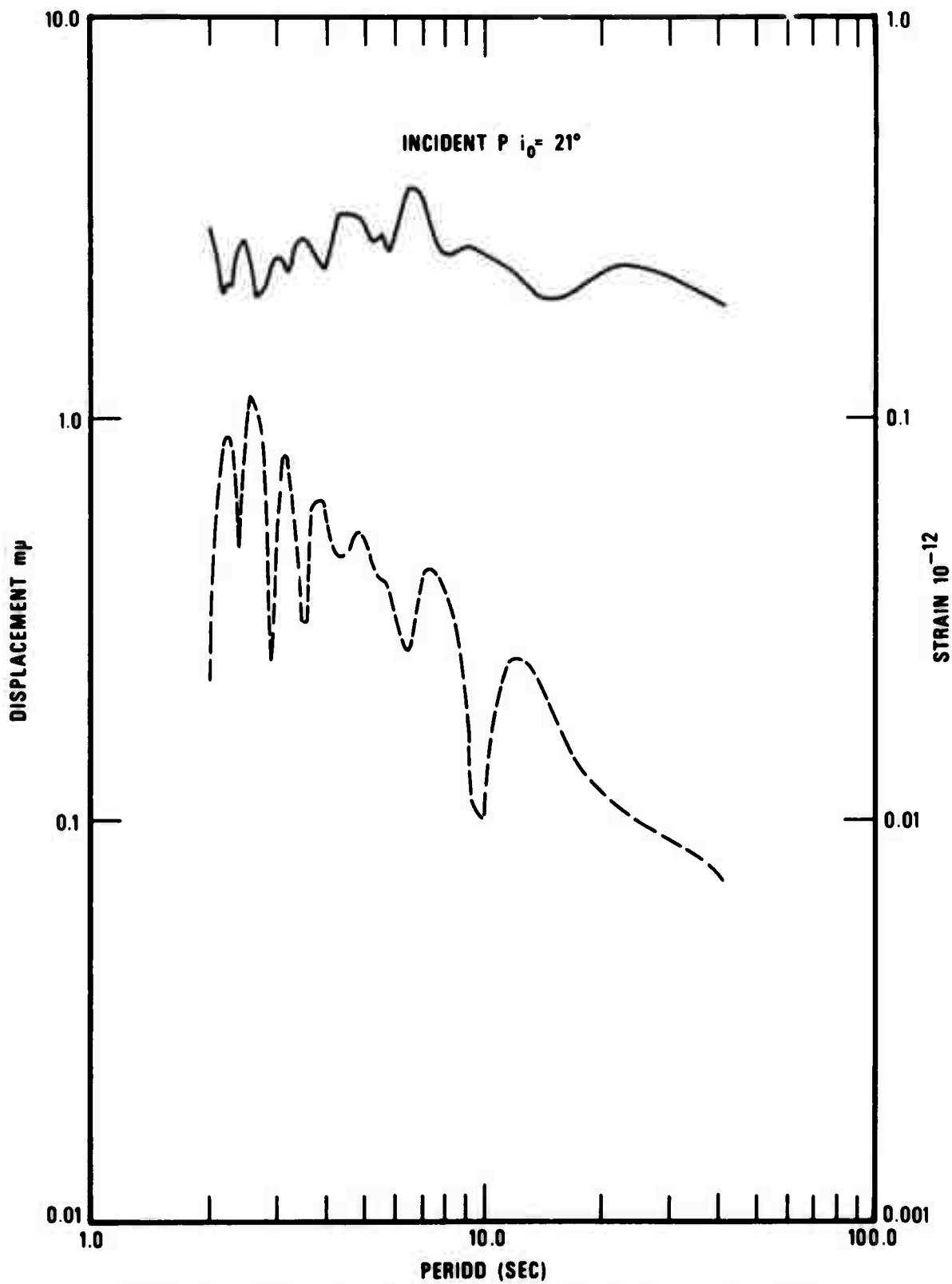


Figure 4. Displacements and strains caused by a P wave incident on crustal model A at an angle of incidence $i_0 = 21^\circ$ (amplitude of incident wave $1 m\mu$).

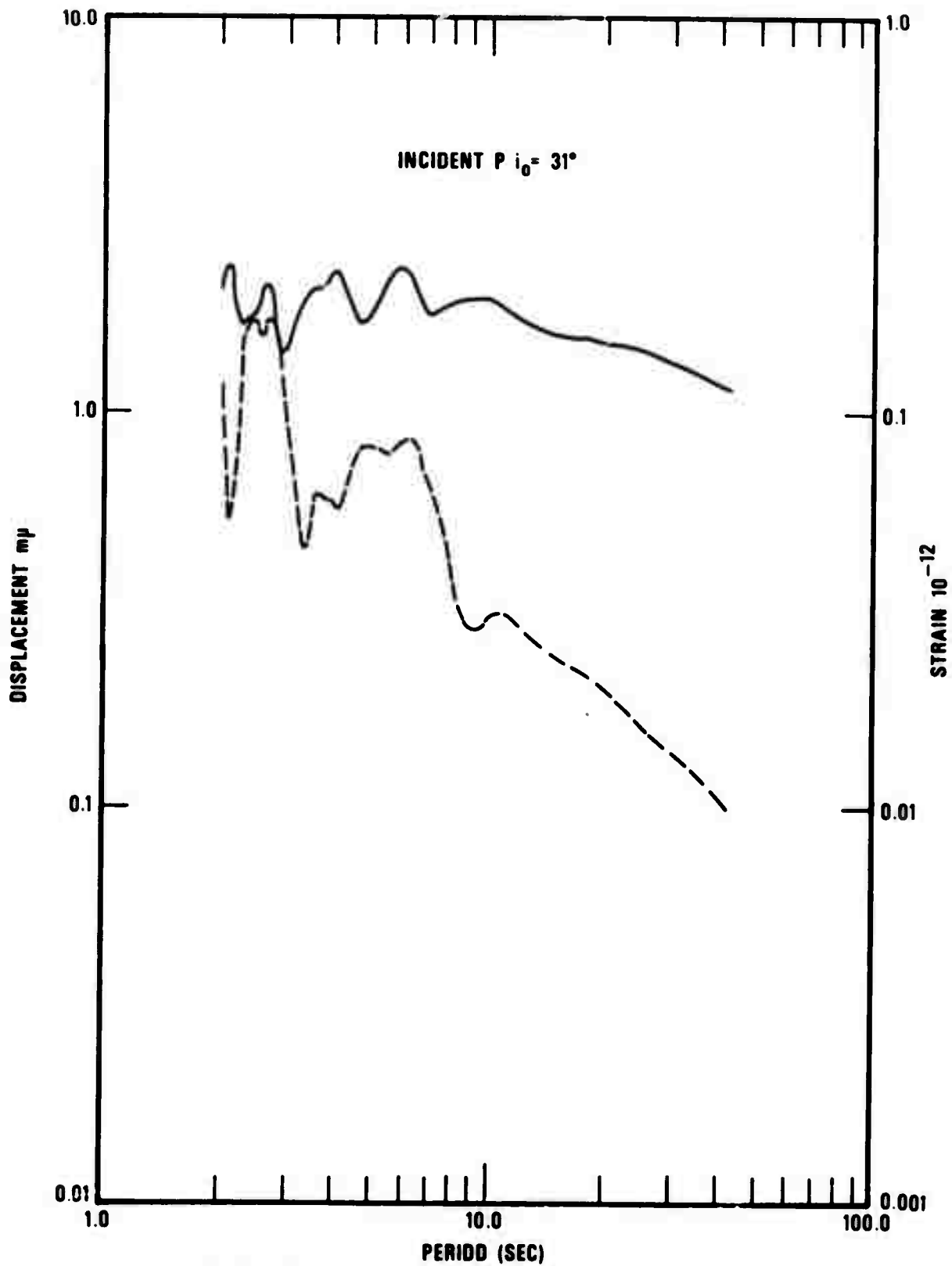


Figure 5. Displacements and strains caused by a P wave incident on crustal model A at an angle of incidence $i_0 = 31^\circ$.

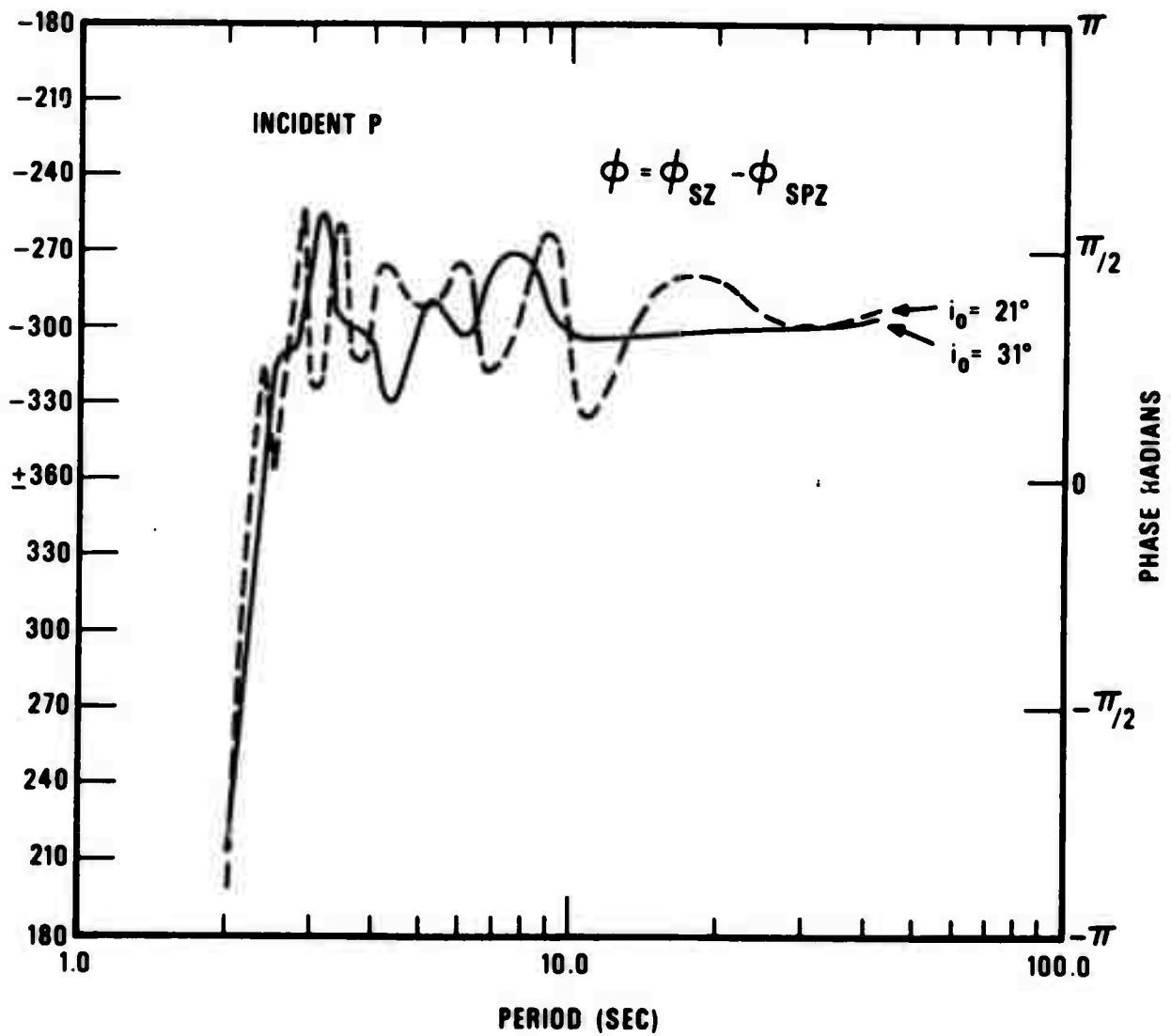


Figure 6. Phase angles between strain and displacement due to P waves incident on crustal model A at angles of incidence 21° and 31° .

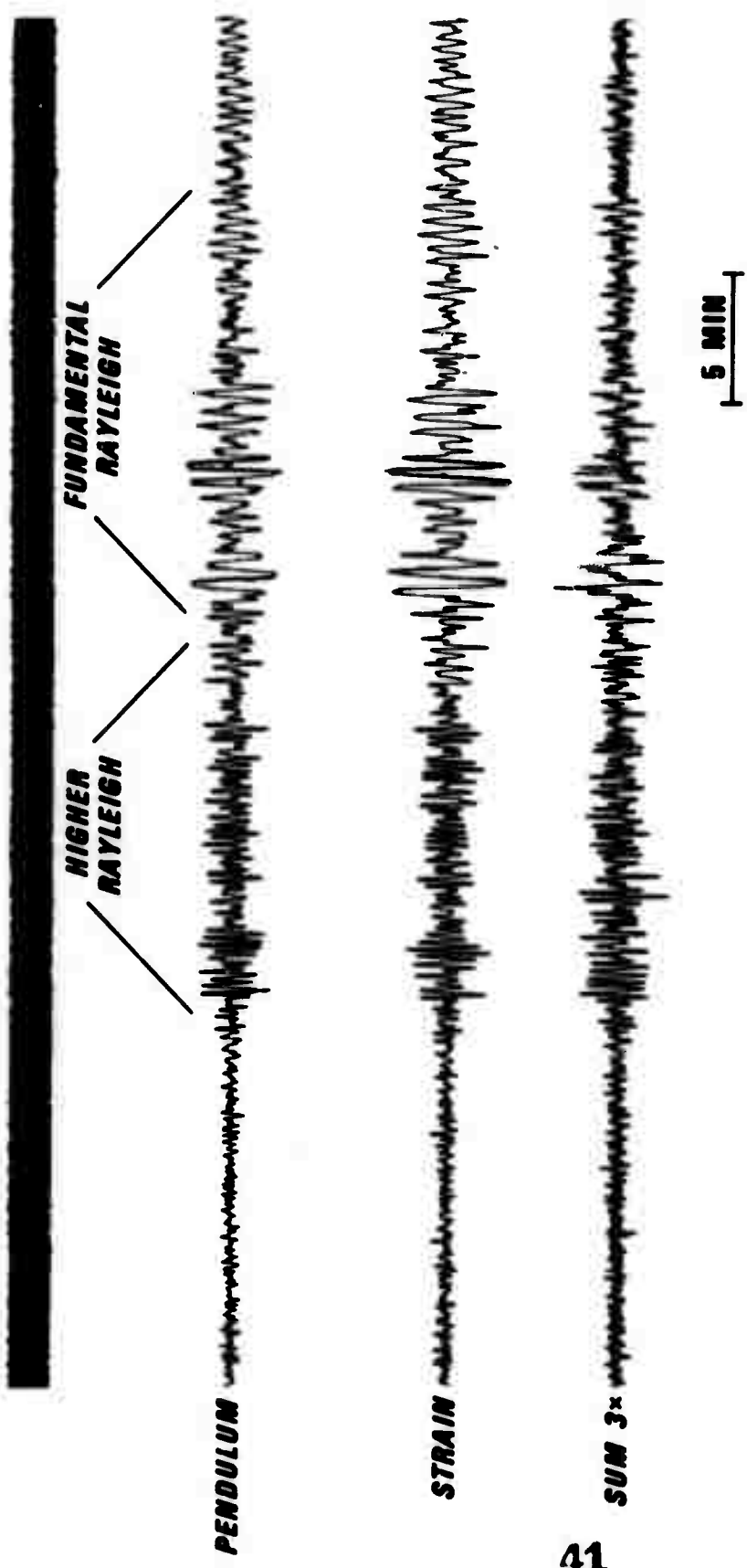


Figure 7. Unequal cancellation of various modes.

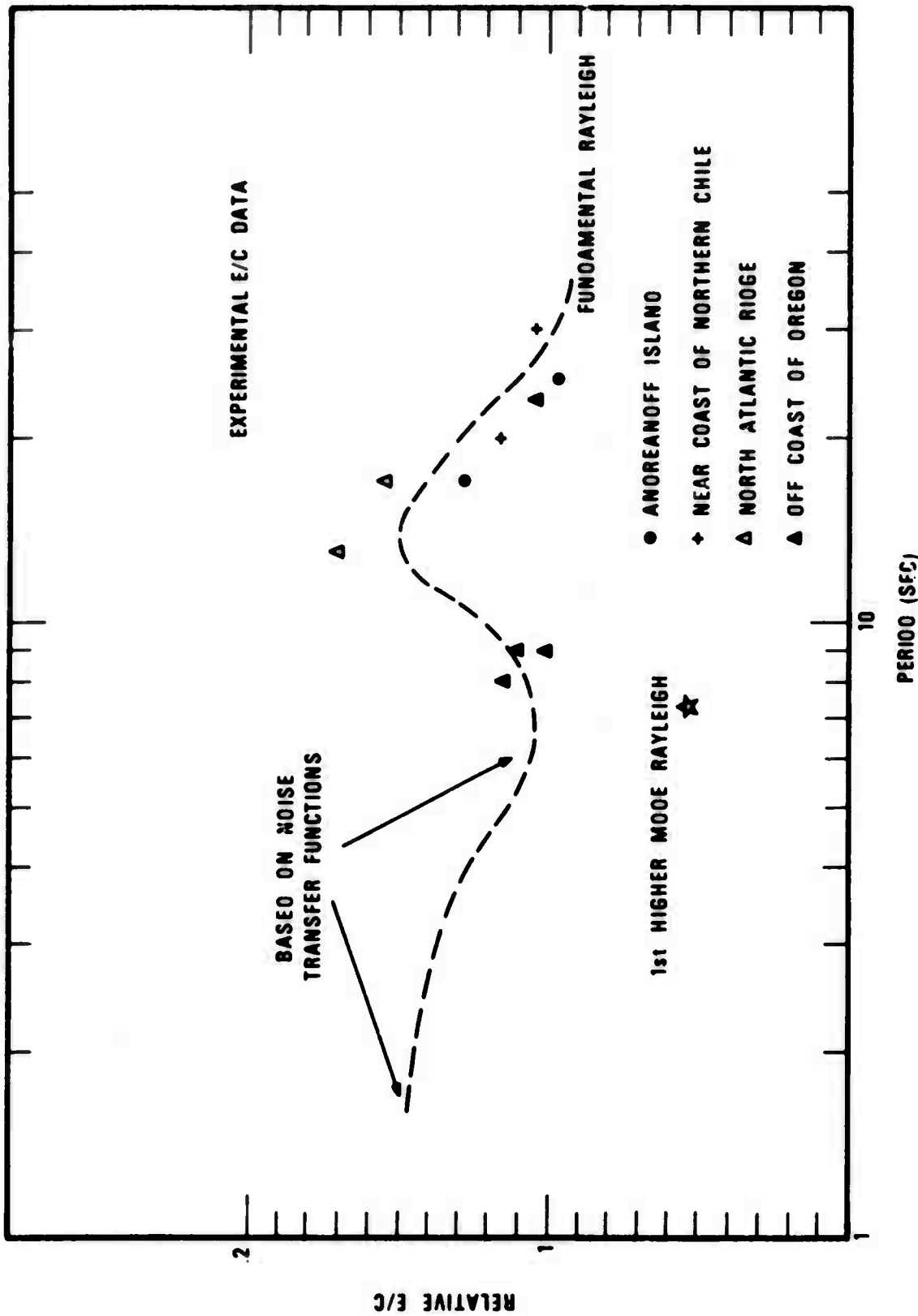


Figure 8a. Ellipticity/phase velocity ratios derived from earthquake surface waves and noise transfer functions.

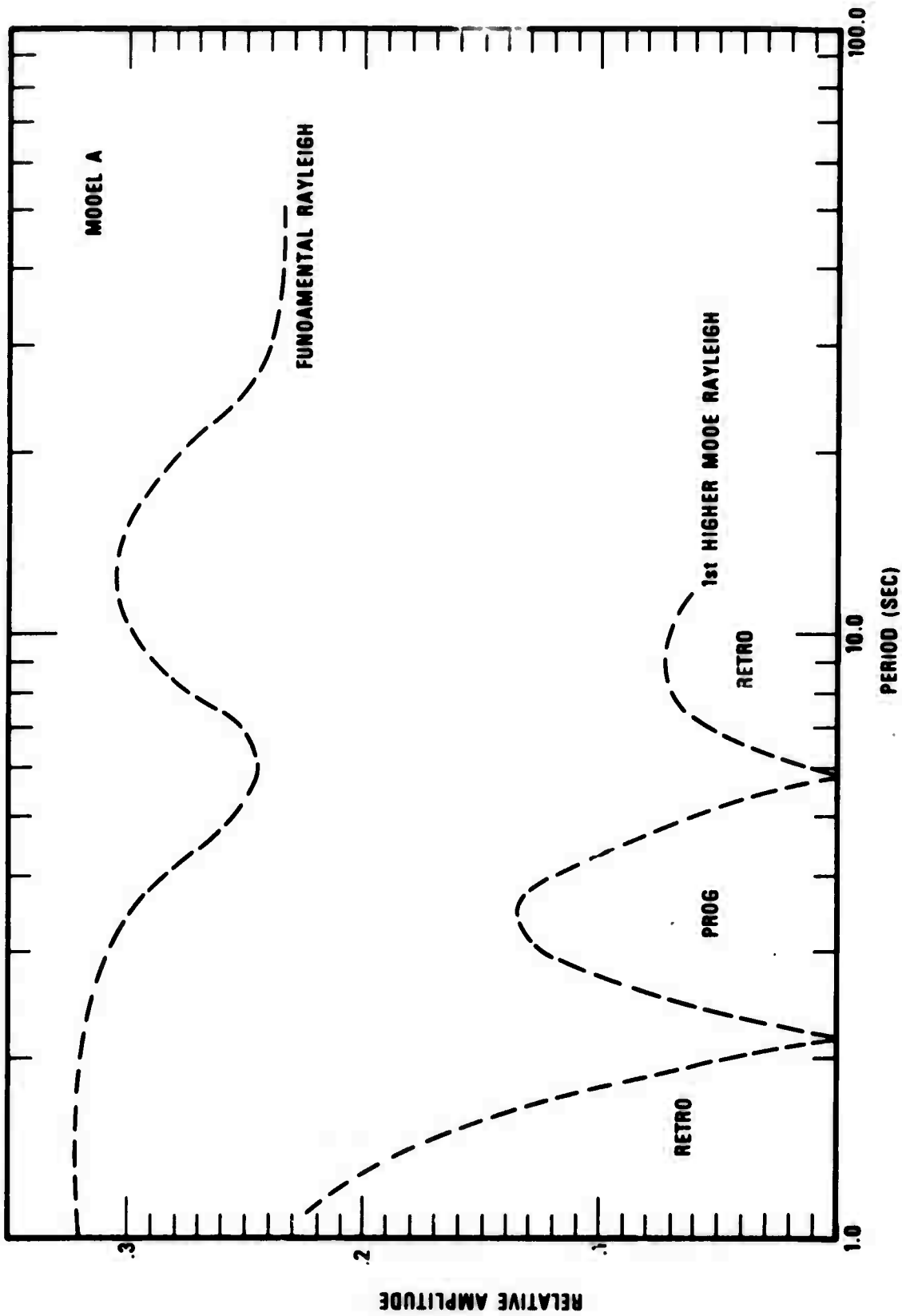


Figure 8b. Ellipticity/phase velocity ratios for crustal model B.

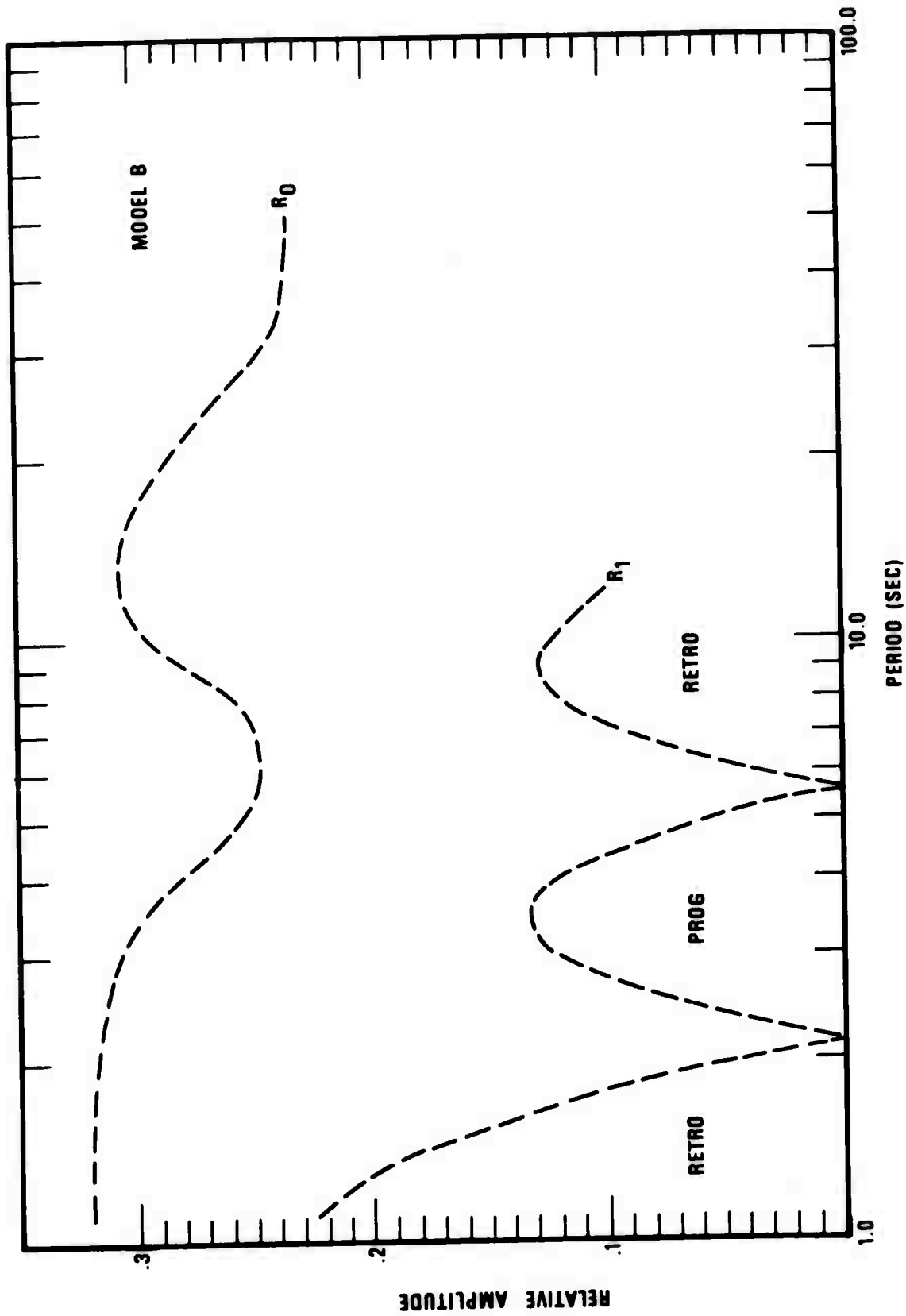


Figure 8c. Ellipticity/phase velocity ratios for crustal model B.

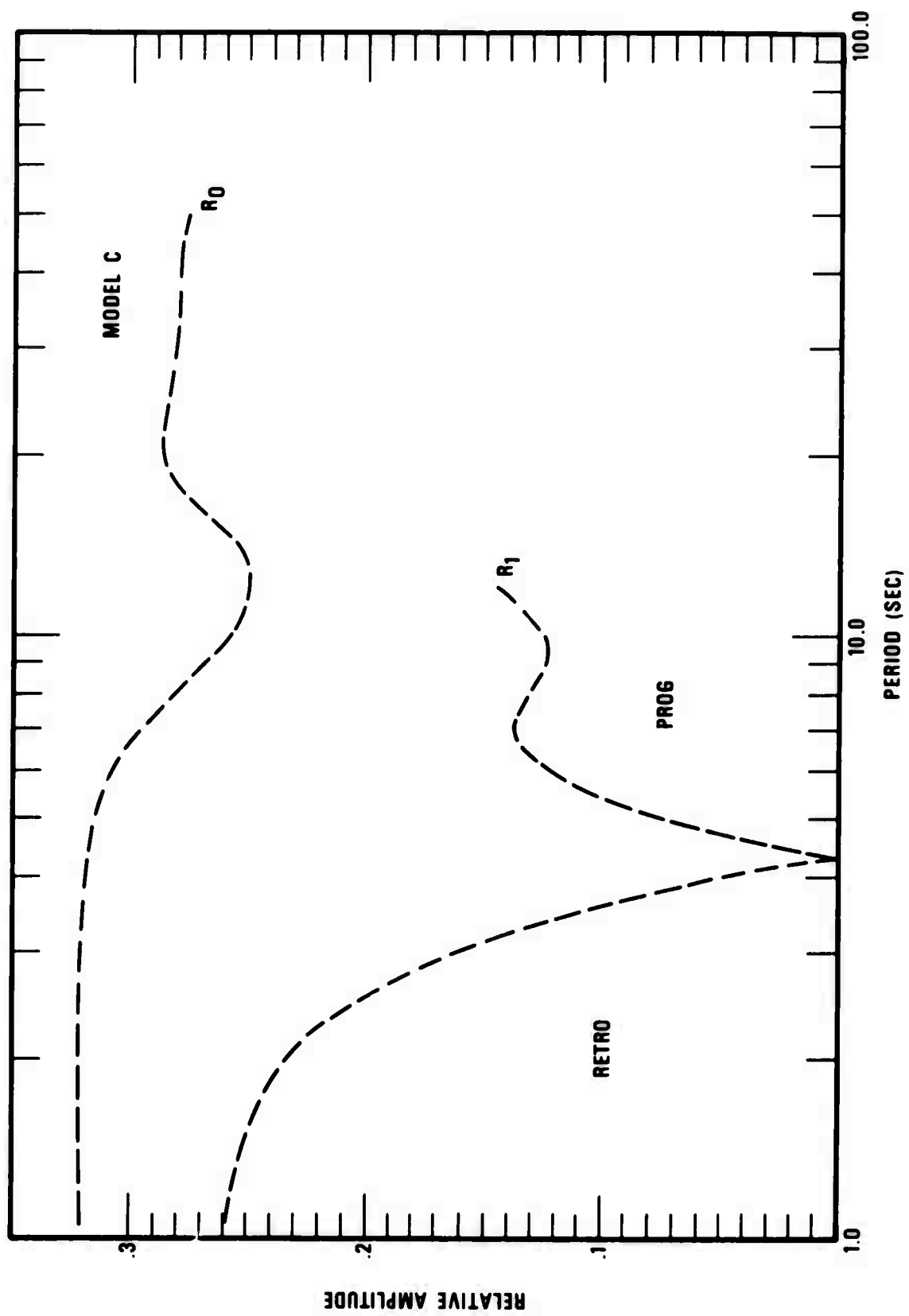


Figure 8d. Ellipticity/phase velocity ratios for crustal model C.

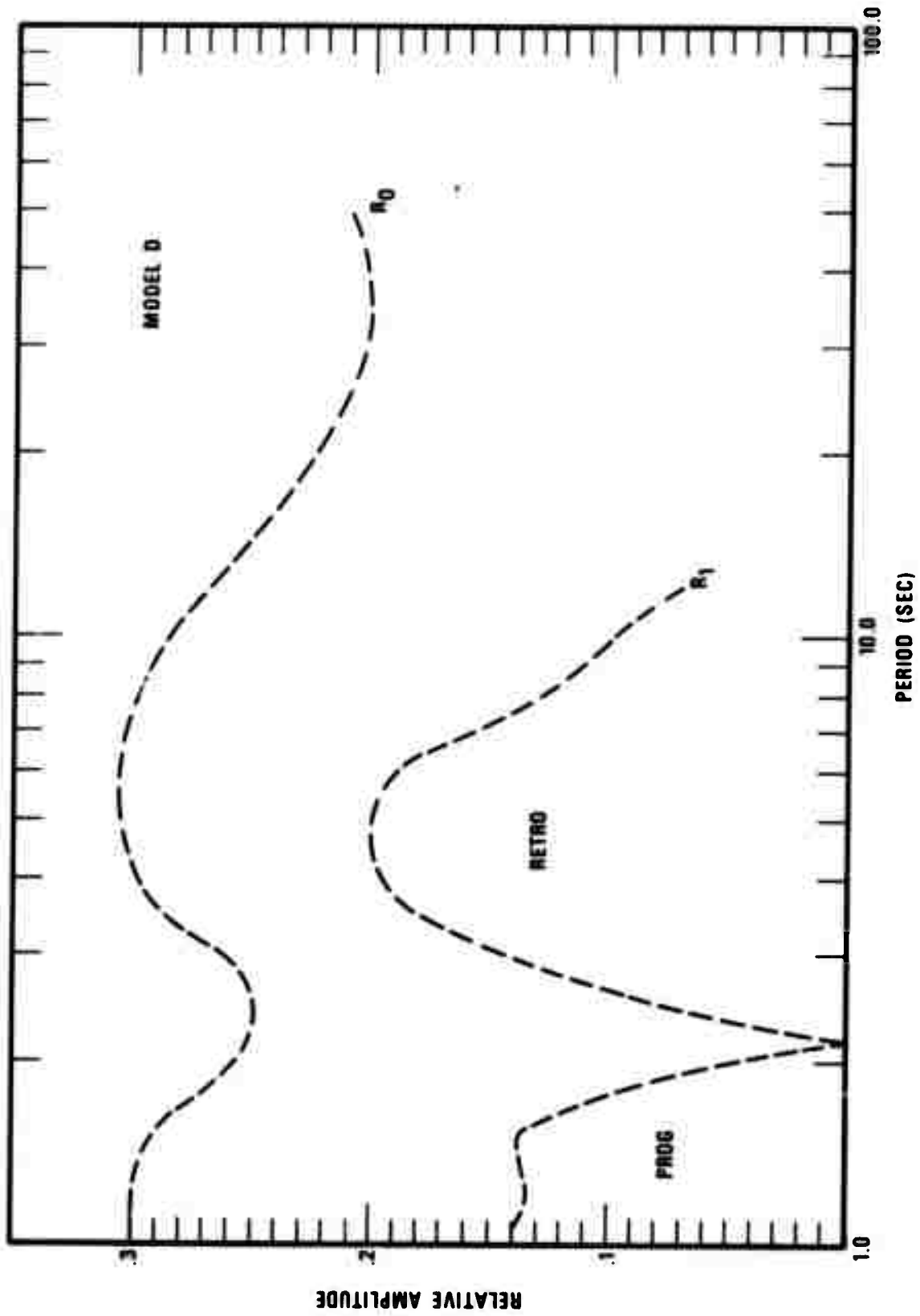


Figure 8e. Ellipticity/phase velocity ratios for crustal model D.

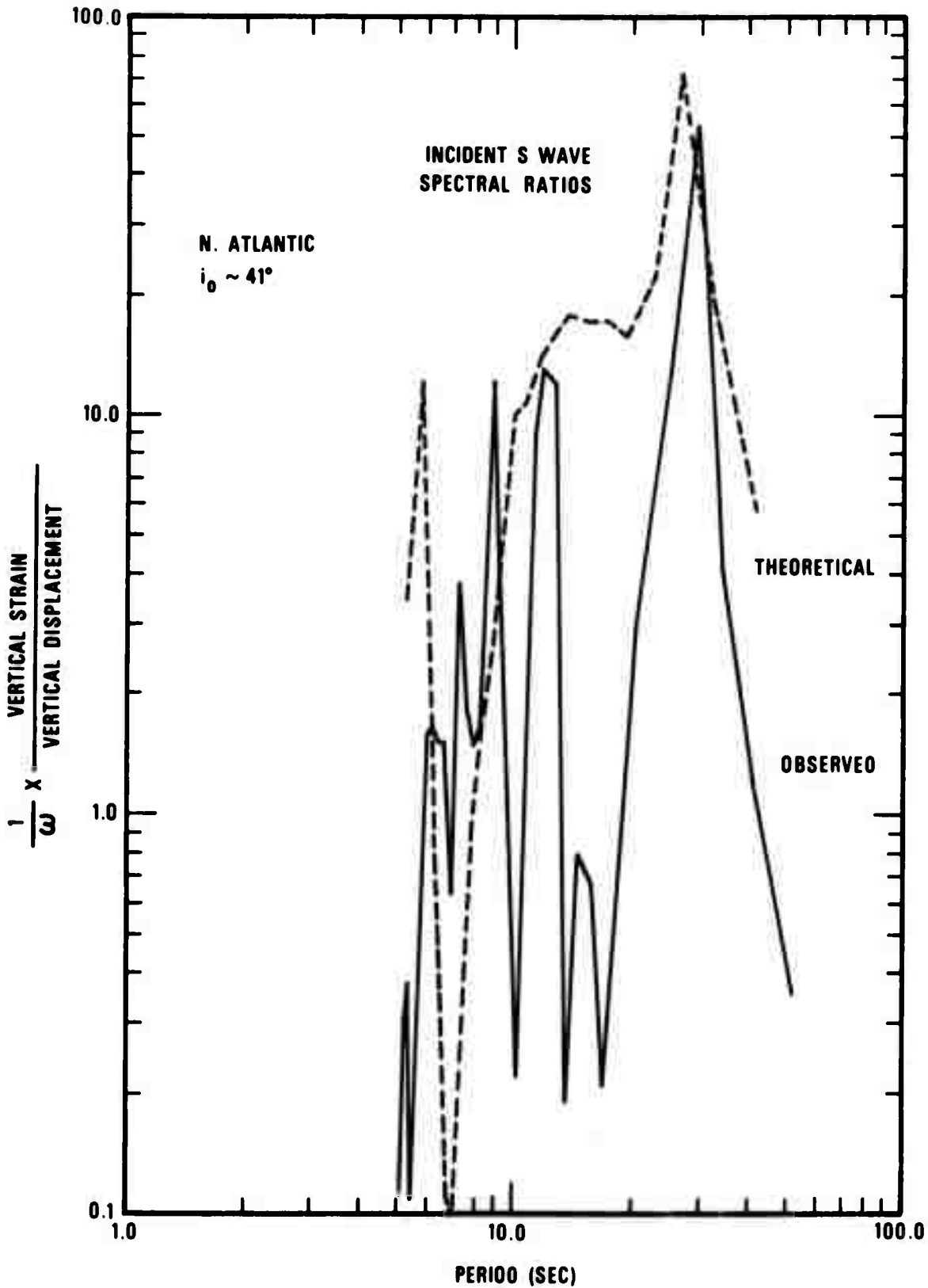


Figure 8f. Theoretical and experimental strain/pendulum spectral ratios for an earthquake S phase.

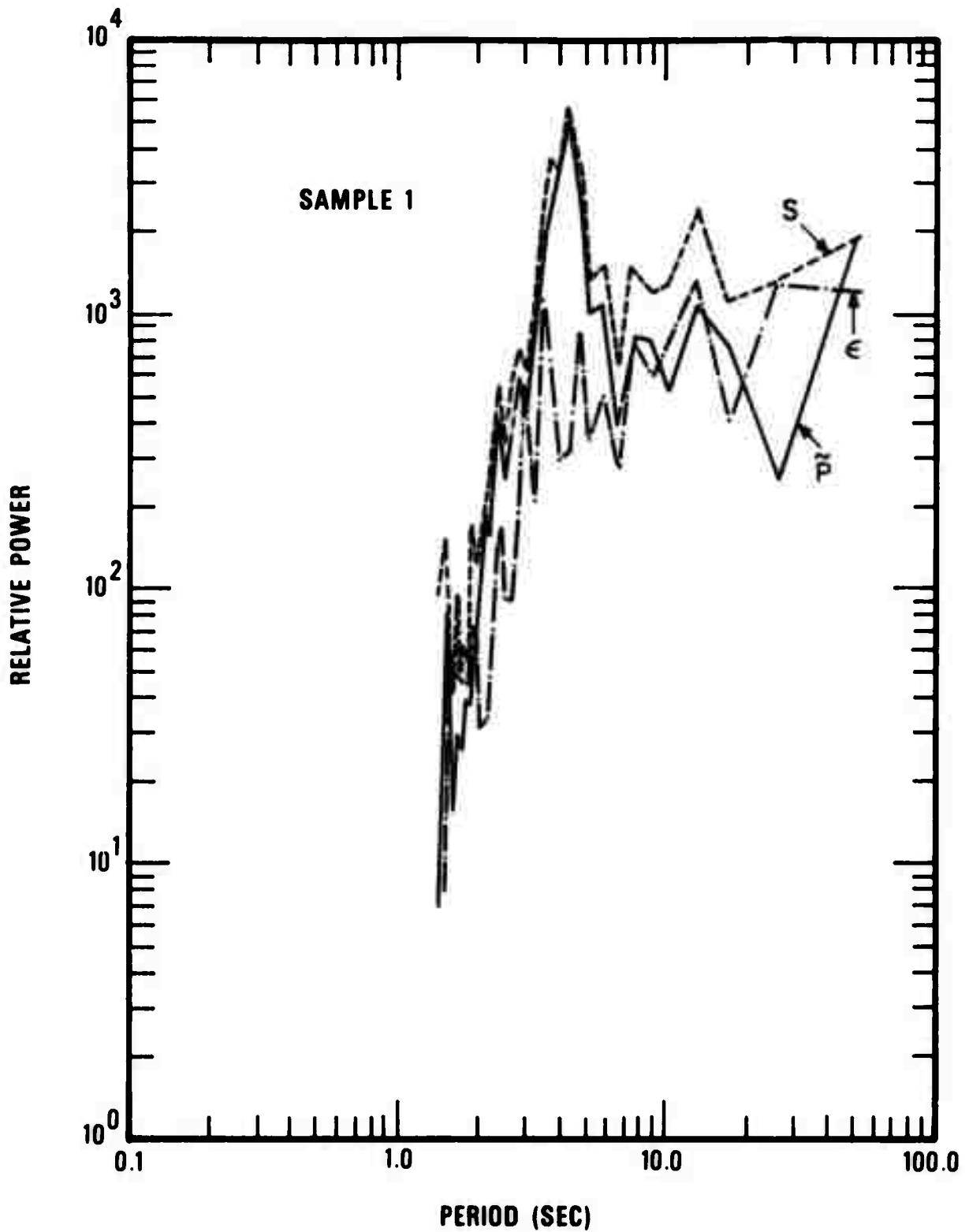


Figure 9. Strain (S), filtered pendulum (\tilde{P}) and error (\tilde{E}) trace power spectra using program INOUT on noise sample 1.

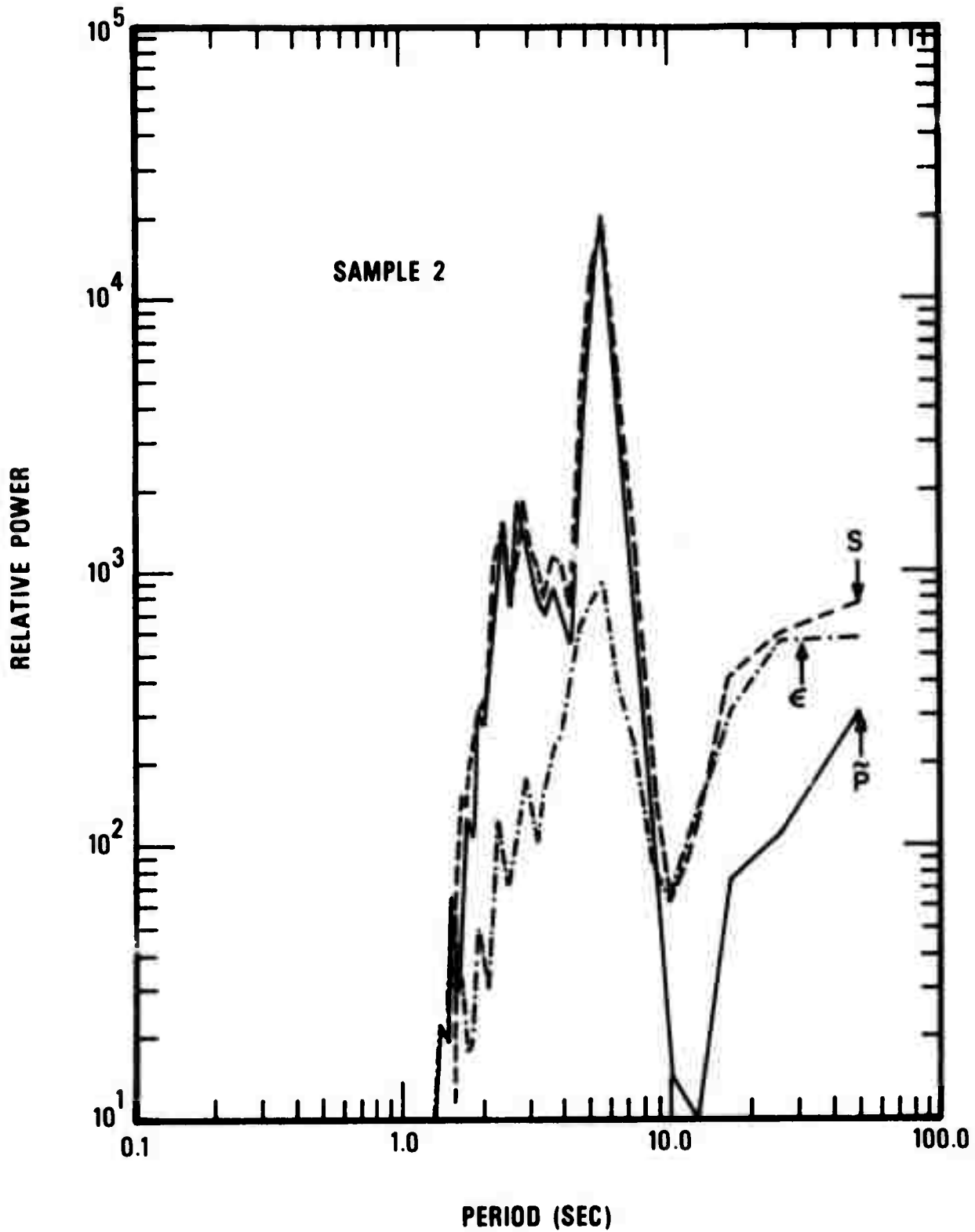


Figure 10. Strain (S), filtered pendulum (\tilde{P}) and error (\tilde{E}) trace power spectra using program INOUT on noise sample 2.

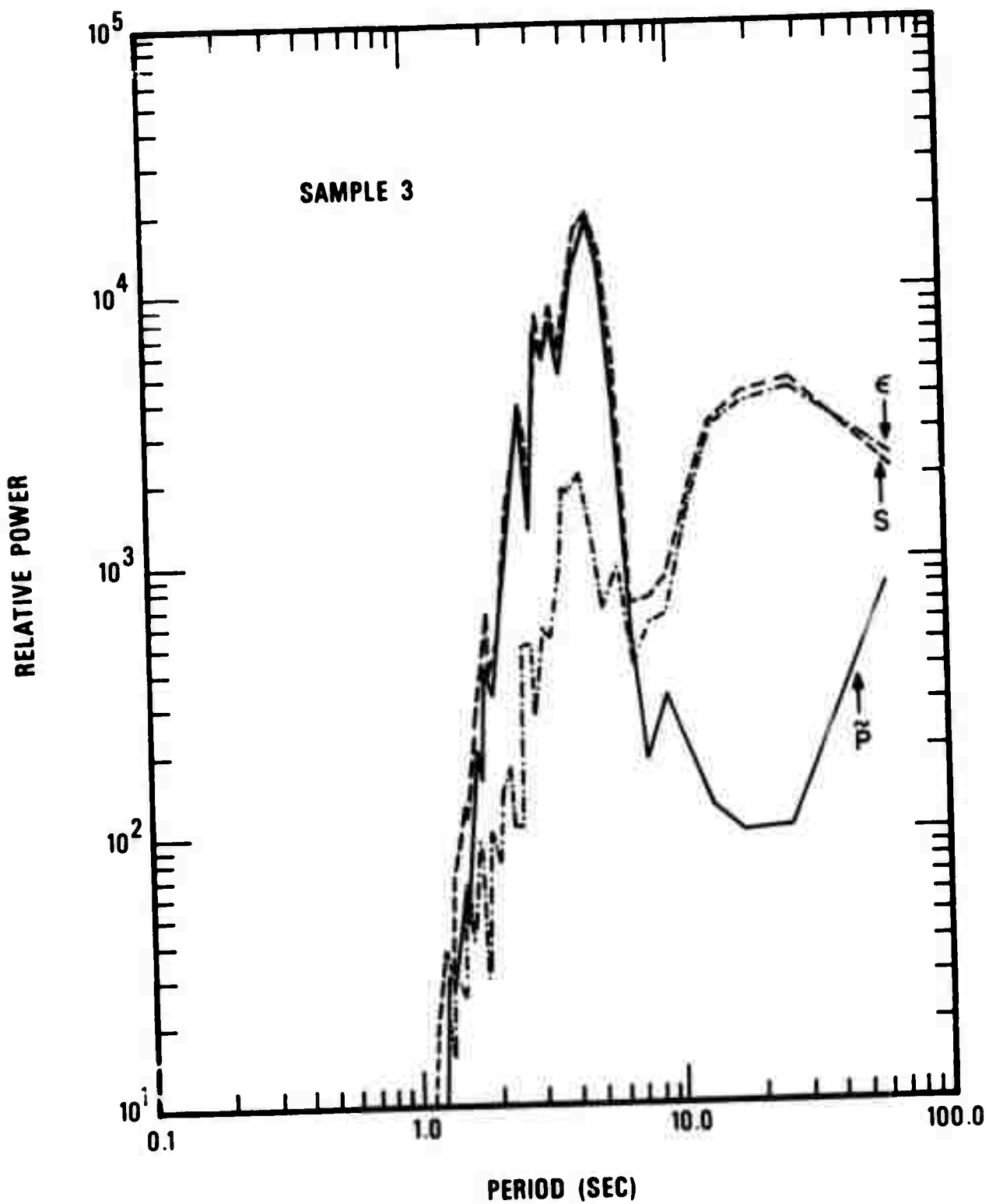


Figure 11. Strain (S), filtered pendulum (\tilde{P}) and error (\tilde{E}) trace power spectra using program INOUT on noise sample.

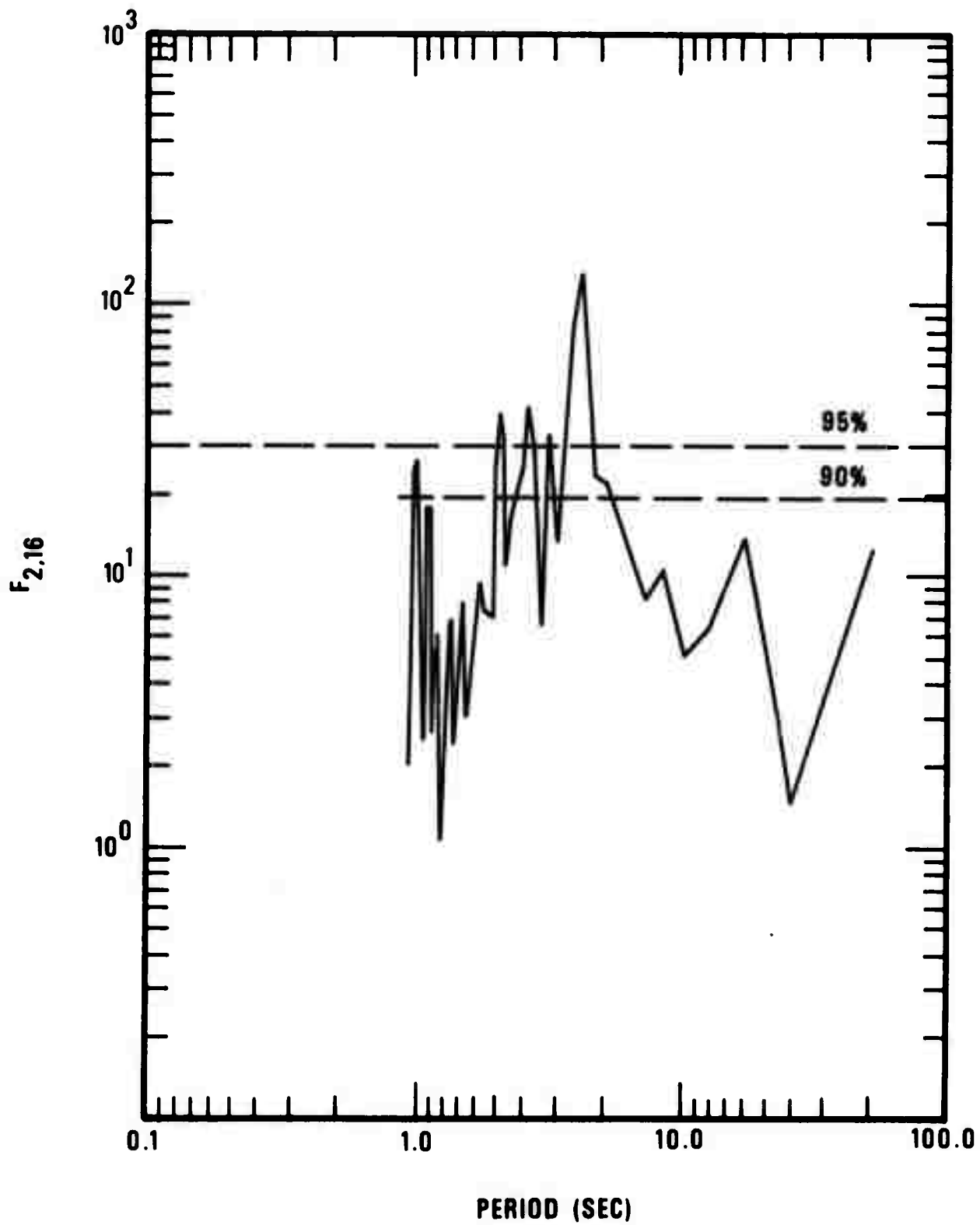


Figure 12. F statistic and confidence limits for the existence of transfer function for noise sample 1.

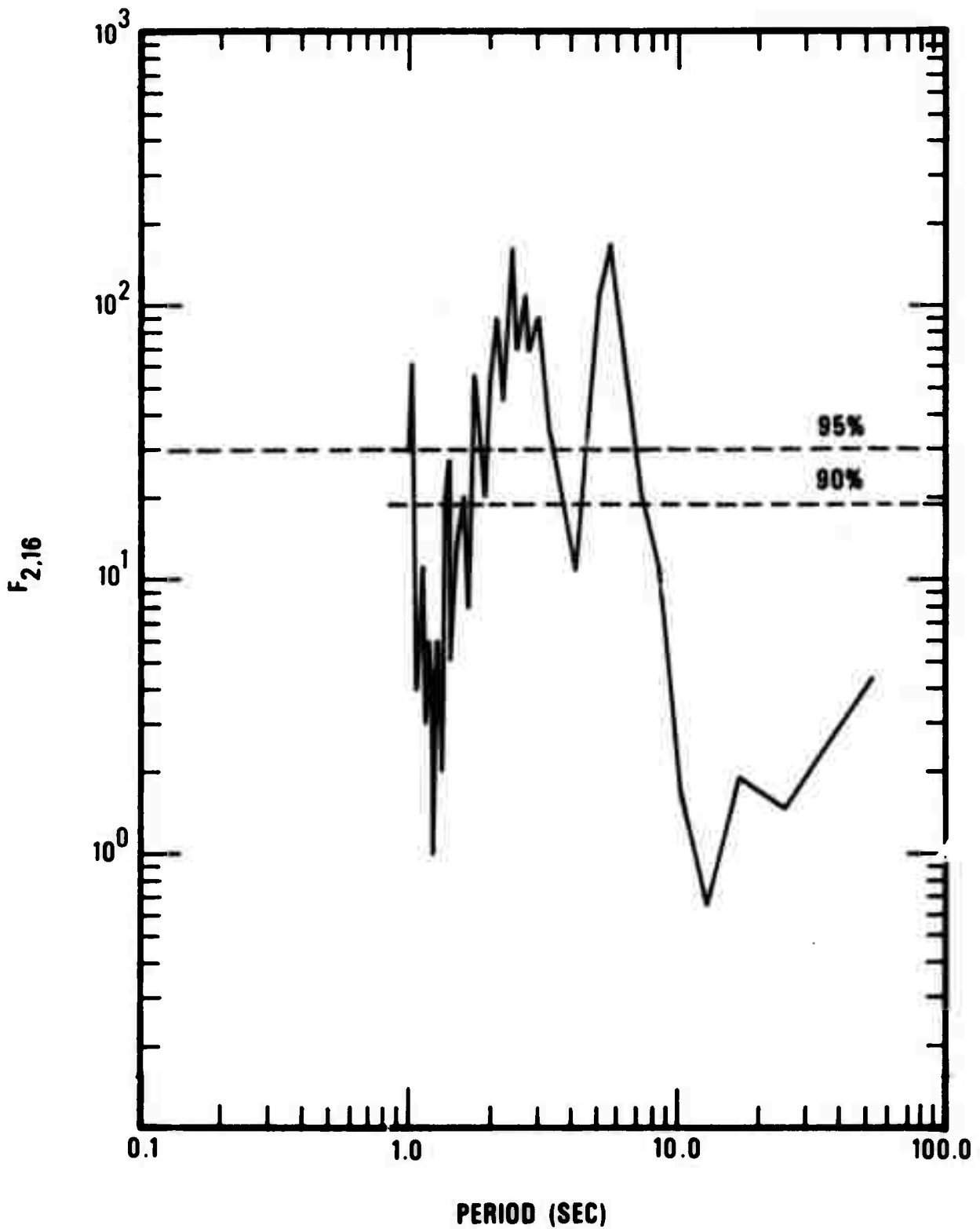


Figure 13. F statistic and confidence limits for the existence of transfer function for noise sample 2.

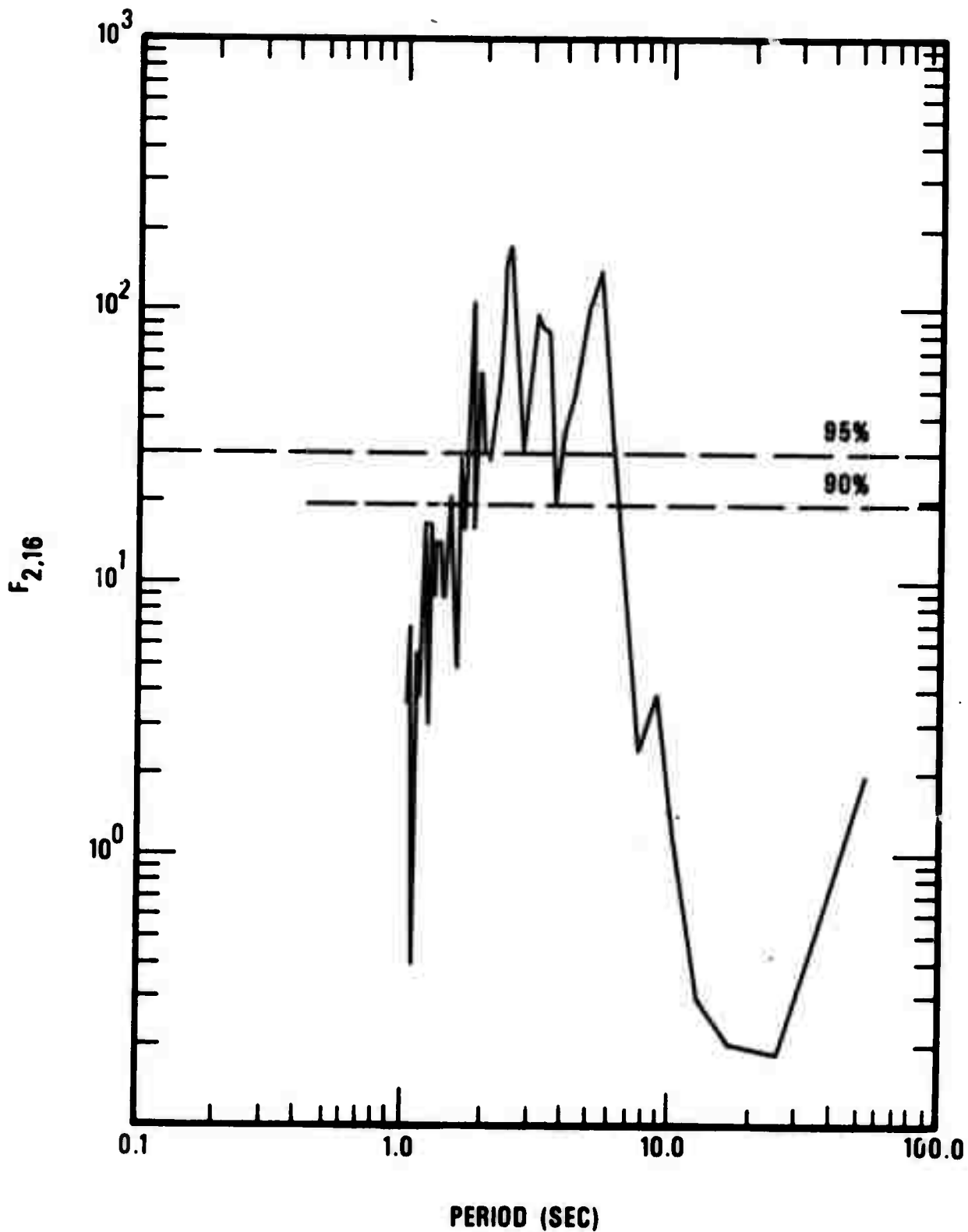


Figure 14. F statistic and confidence limits for the existence of transfer function for noise sample 3.

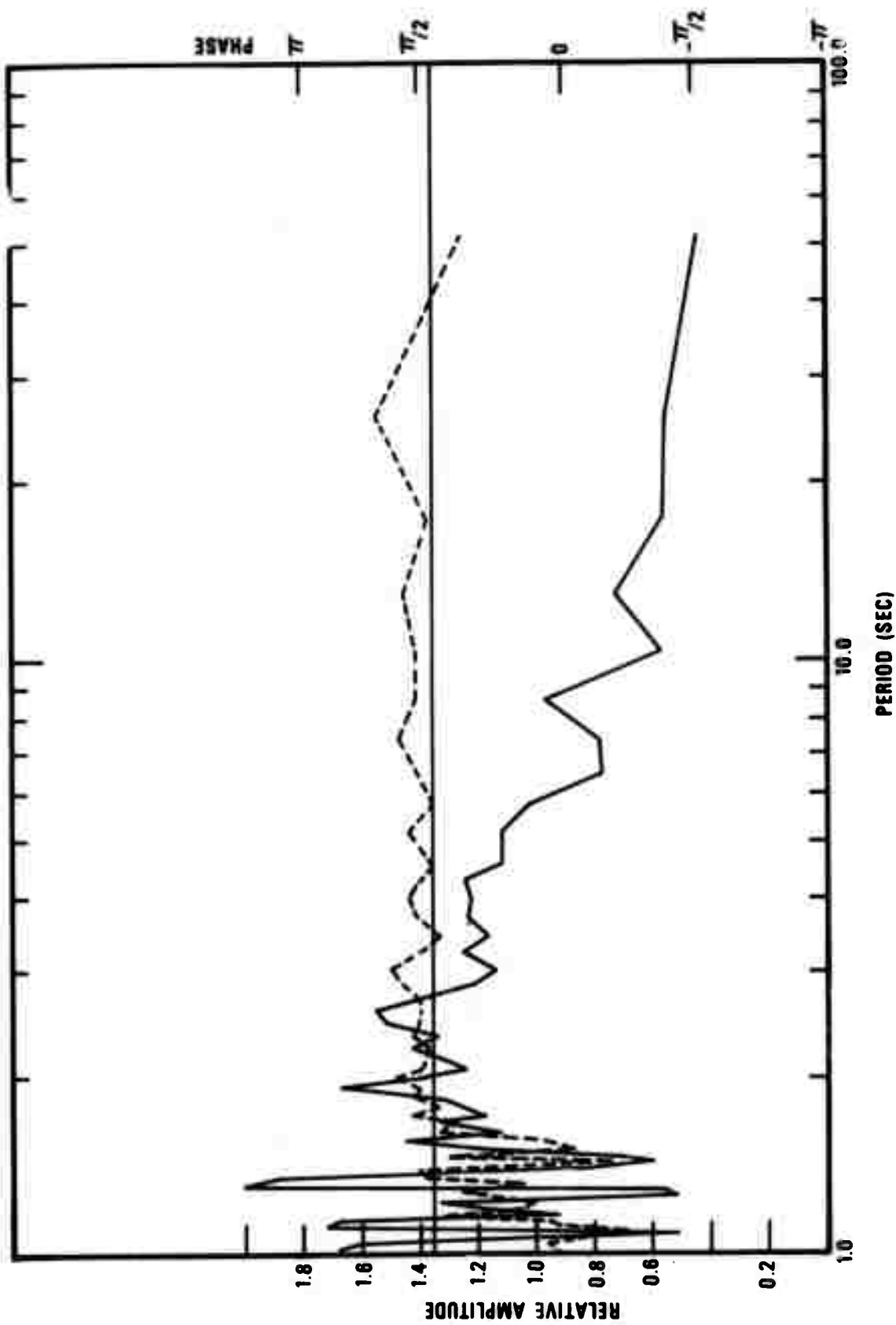


Figure 15. Pendulum to strain noise transfer functions for noise sample 1 using program INOUT.

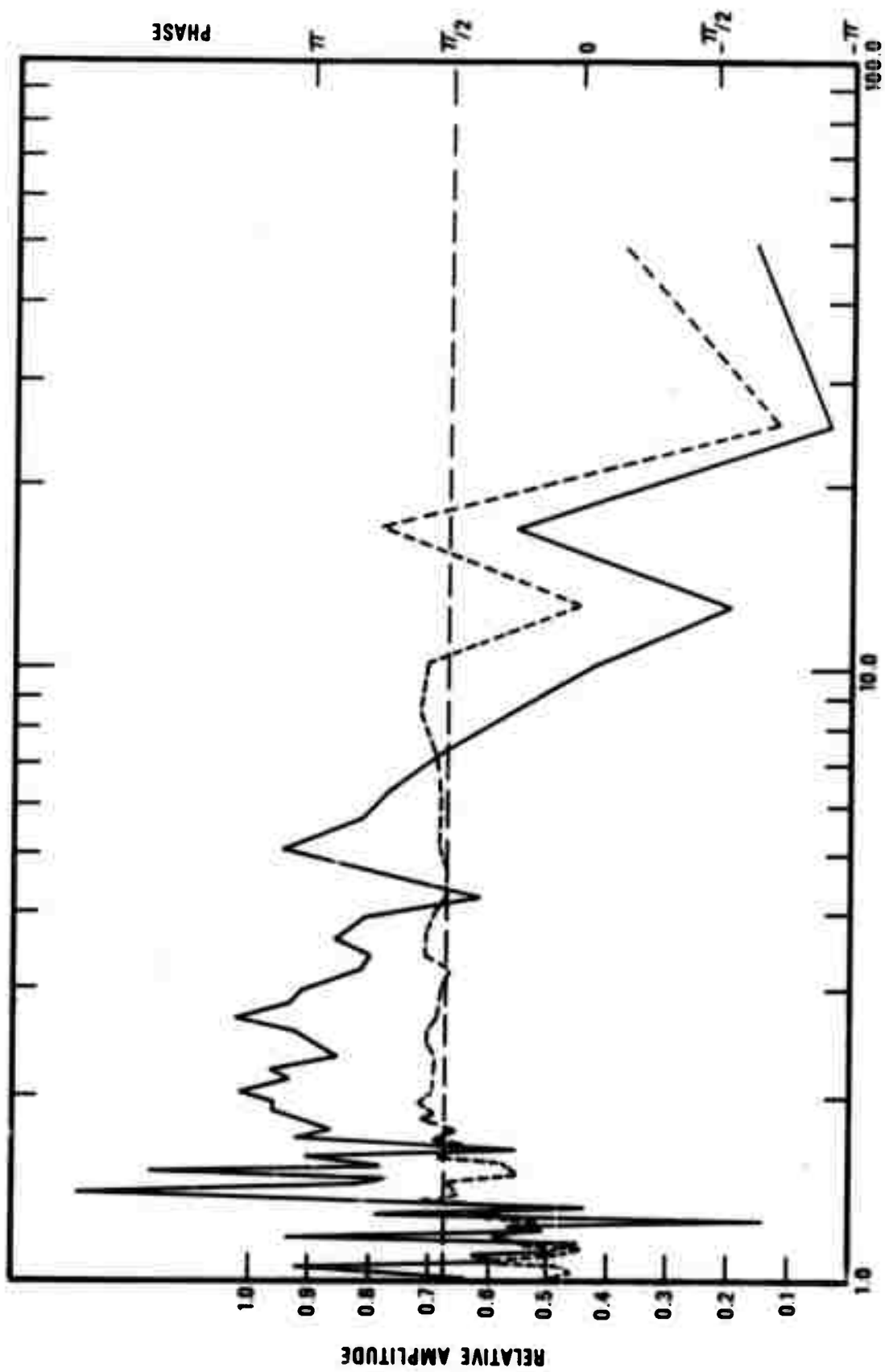


Figure 16. Pendulum to strain noise transfer functions for noise sample 2 using program INOUT.

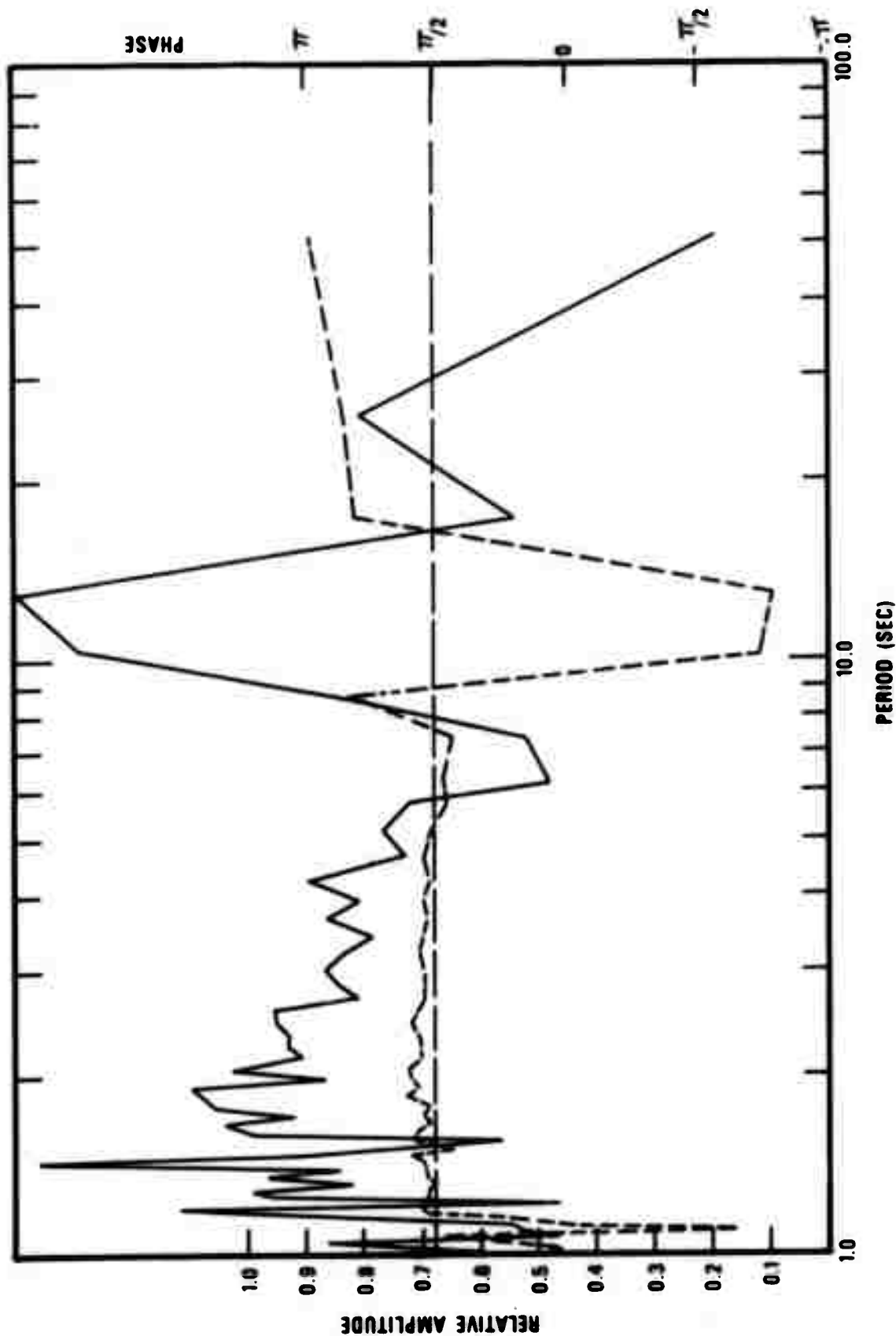
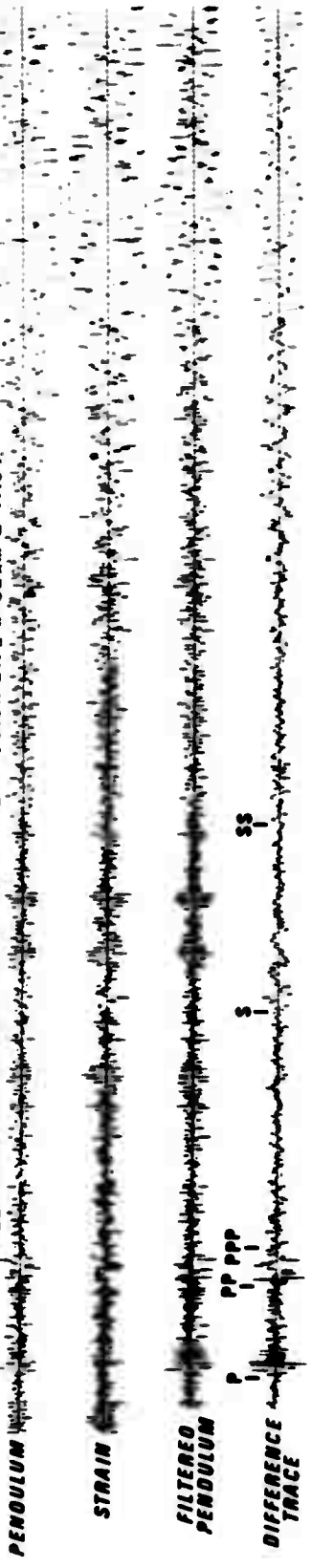


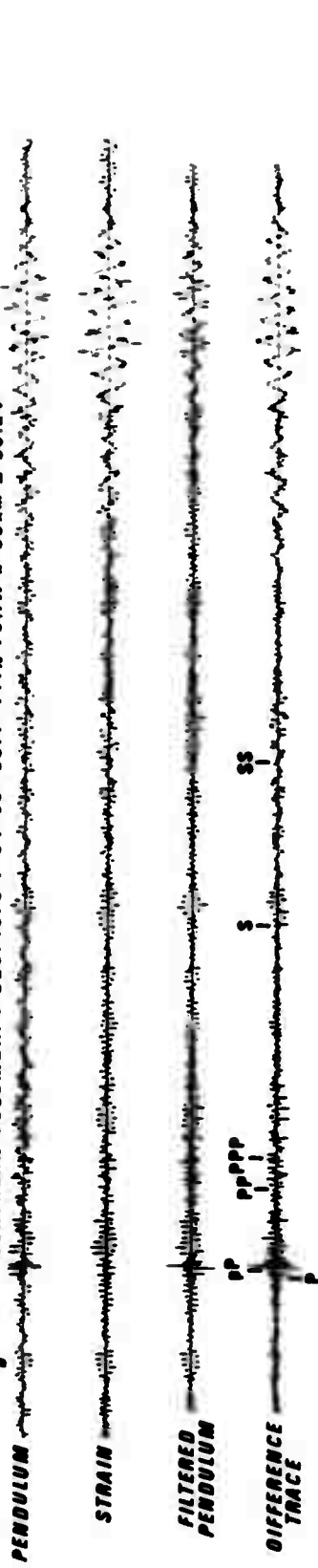
Figure 17. Pendulum to strain noise transfer functions for noise sample 3 using program INOUT.

$M_b = 5.0$

GREENLAND SEA 26 OCT. 1970 T=20 53°32.4' 79.8N 2.7E h=32km A=01.50°



$M_b = 5.7$ NORTHERN COLOMBIA 3 DEC. 1970 T=04 50°53.4' 7.4N 70.1W h=30km A=39.24°



$M_b = 5.0$ NEAR COAST OF NORTHERN CHILE 4 DEC. 1970 T=17 00°40.7' 23.1S 70.1W h=30km A=00.95°

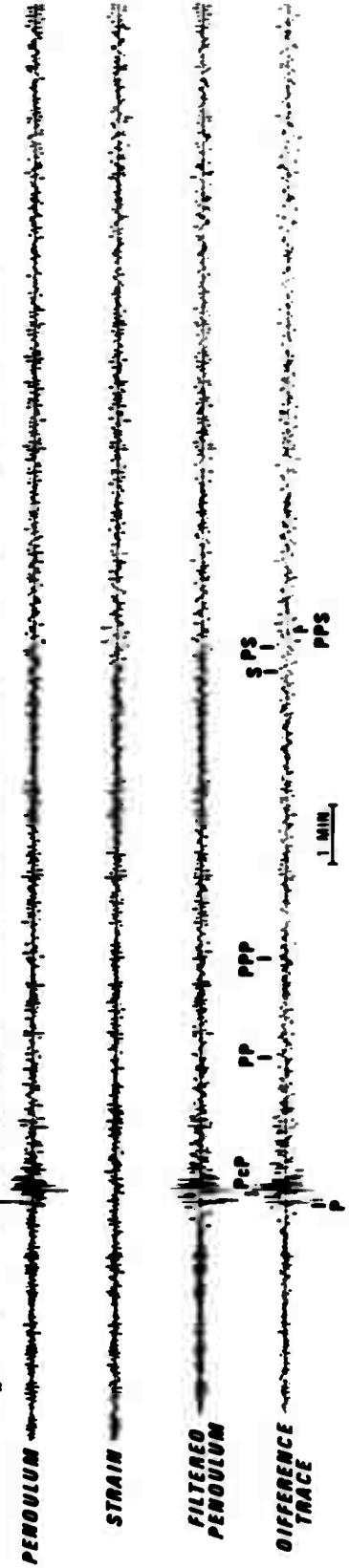


Figure 18. Traces processed by program INOUT. Amplitude is relative.

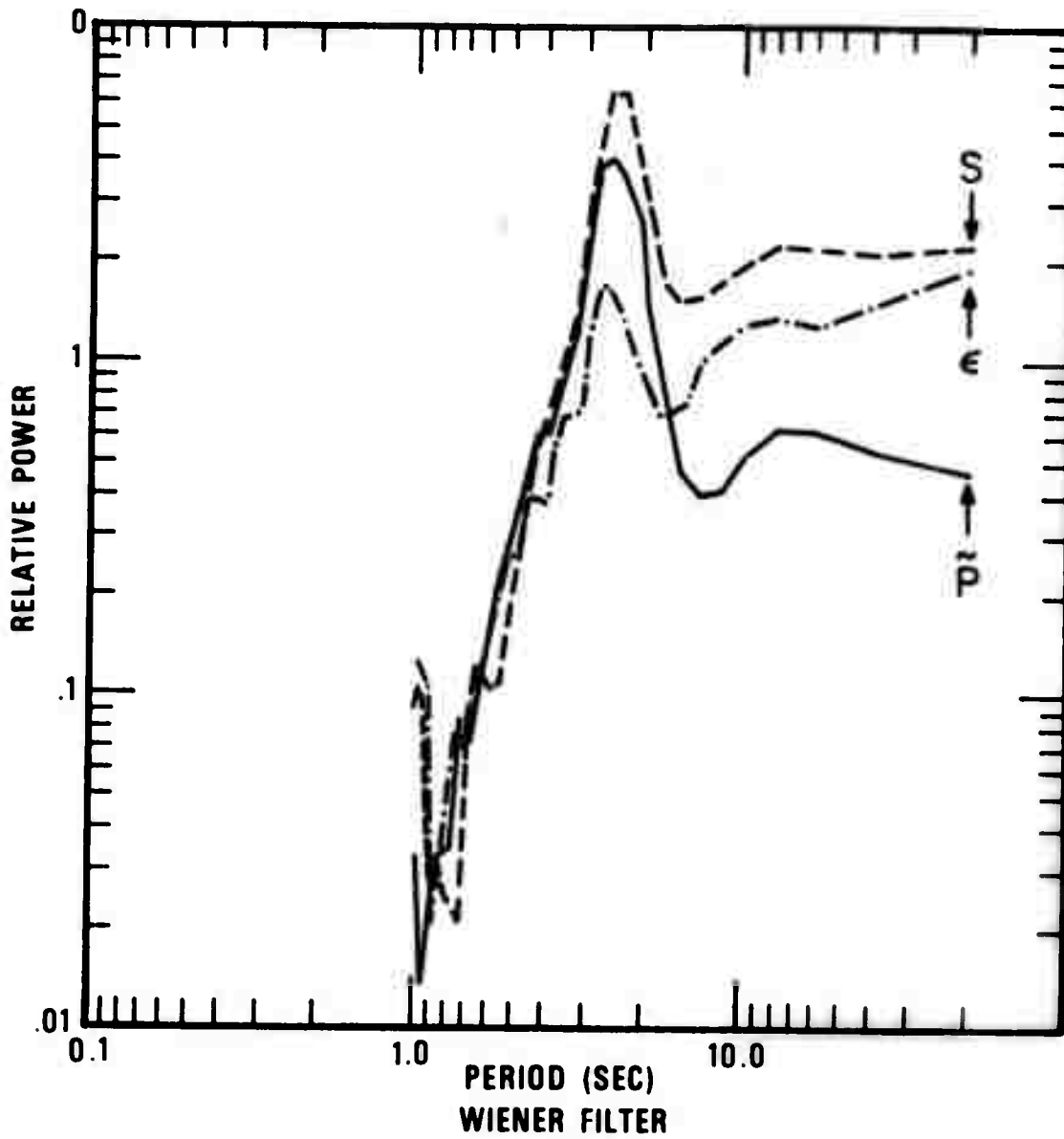


Figure 19. Strain (S), filtered pendulum (\tilde{P}) and error (\tilde{E}) trace power spectra for one sided 64 pt Wiener filter on noise sample 1.

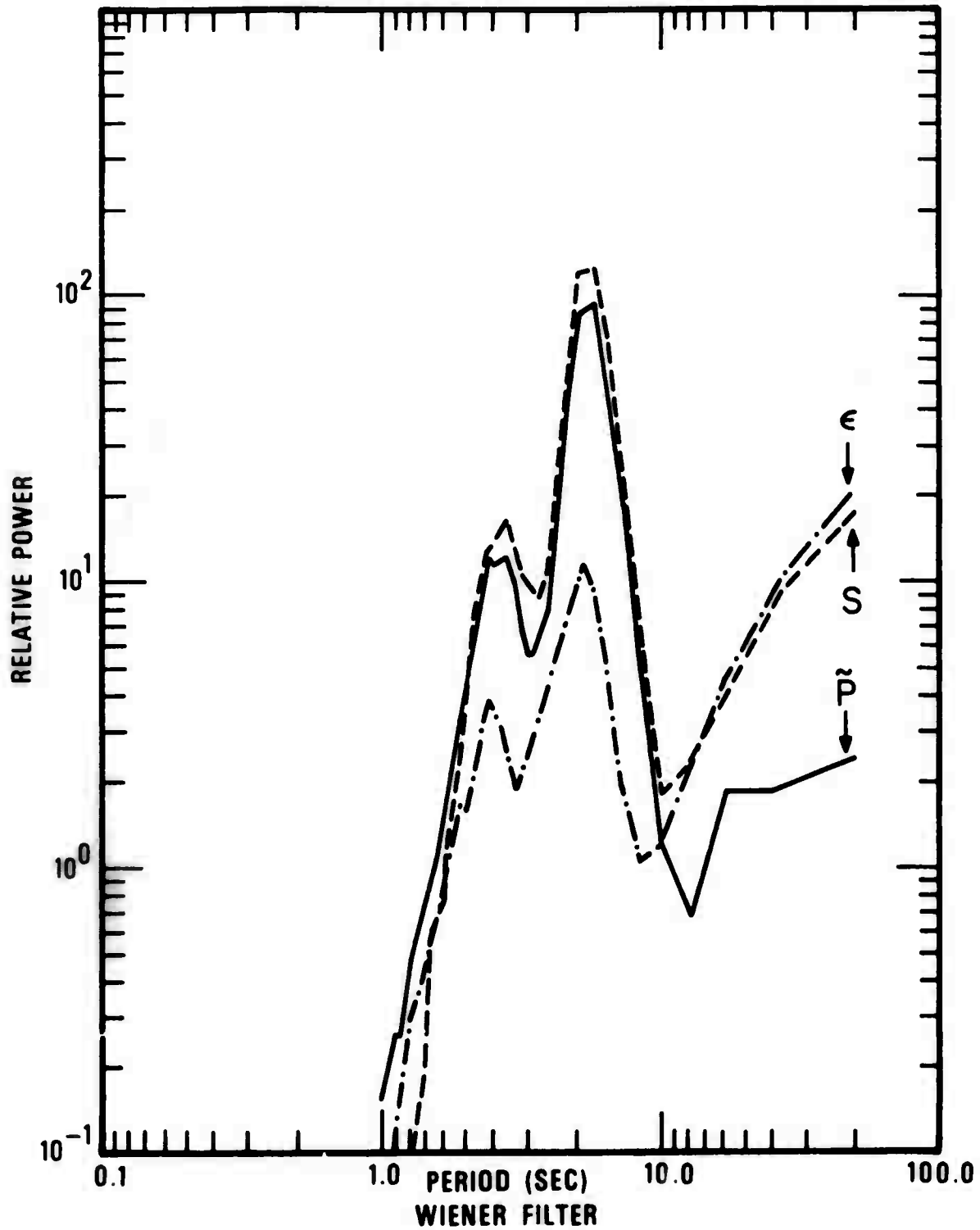


Figure 20. Strain (S), filtered pendulum (\tilde{P}) and error ($\tilde{\epsilon}$) trace power spectra for one sided 64 pt Wiener filter on noise sample 2.

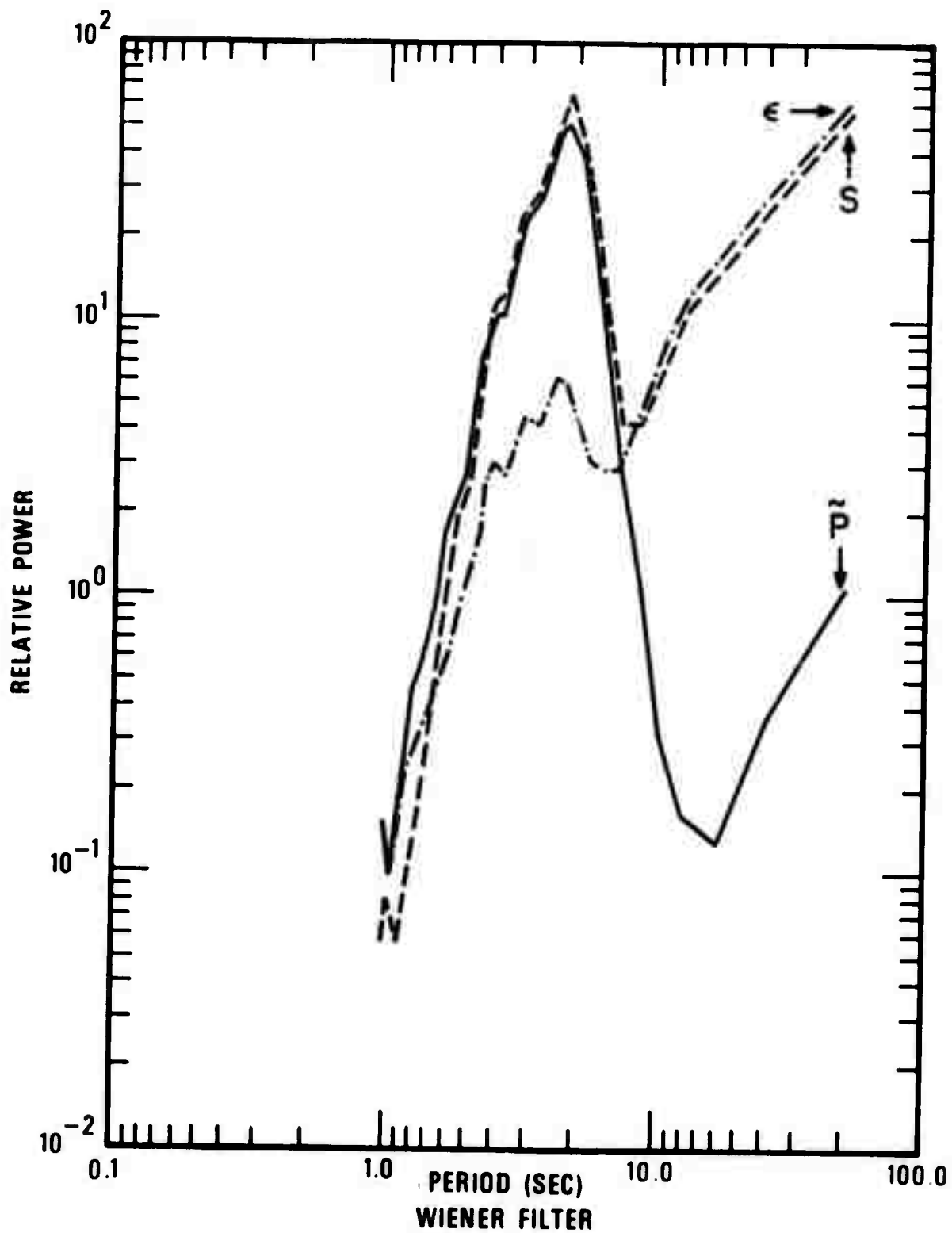


Figure 21. Strain (S), filtered pendulum (\bar{P}) and error ($\bar{\epsilon}$) trace power spectra for one sided 64 pt Wiener filter on noise sample 3.

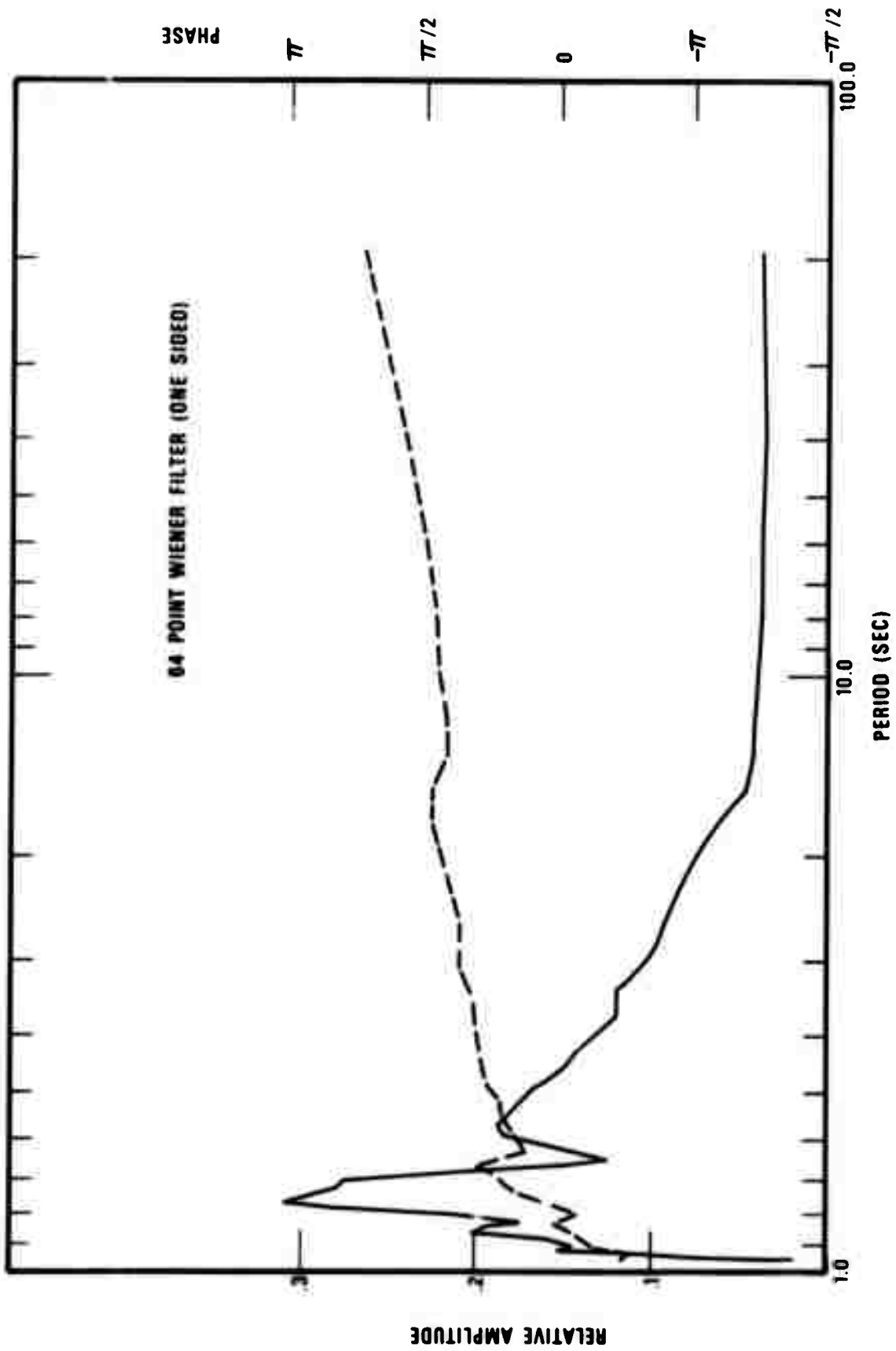


Figure 22. Response of 64 pt Wiener filters designed for noise sample 1 pendulum trace.

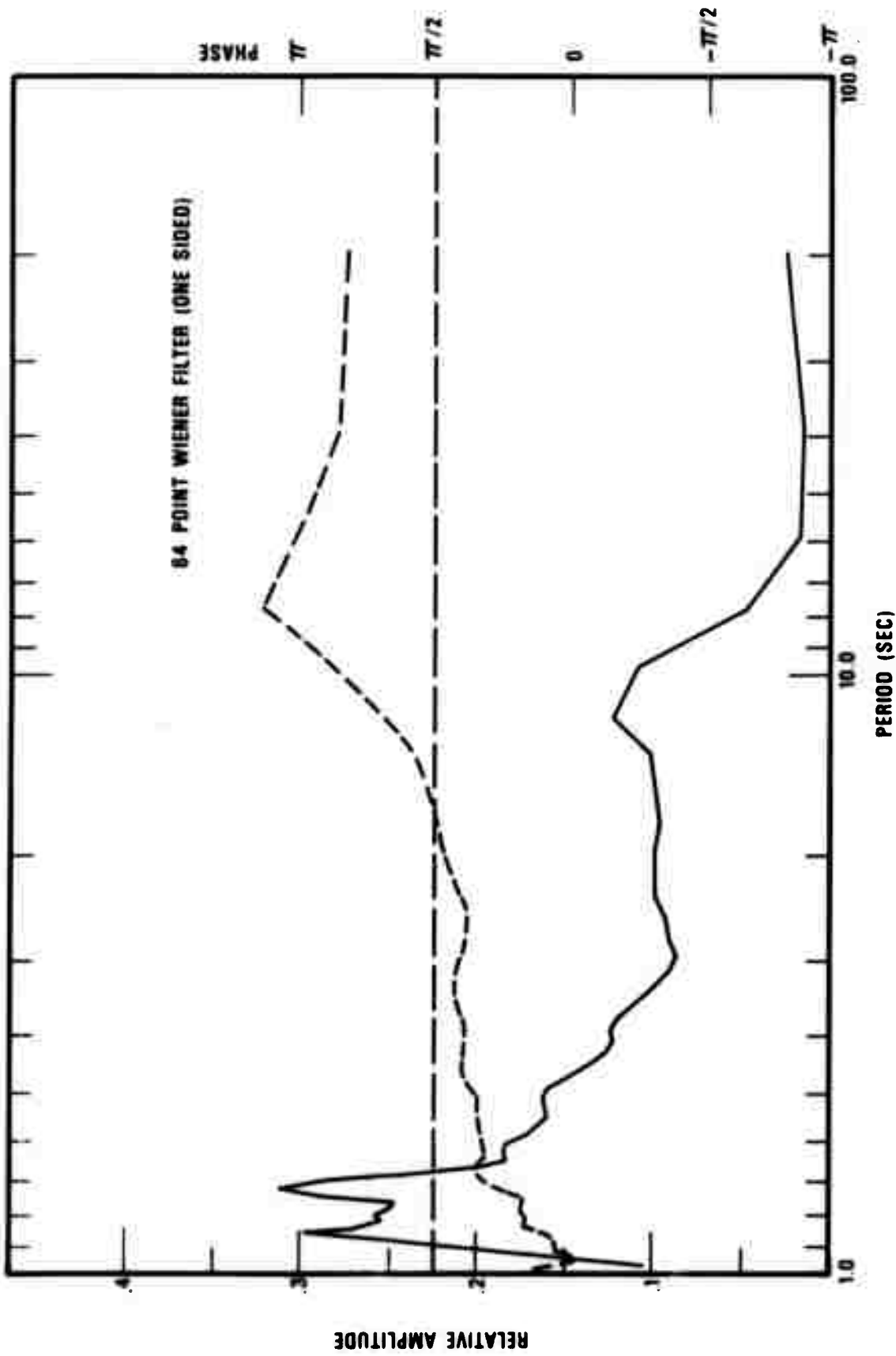


Figure 23. Response of 64 pt Wiener filters designed for noise sample 2 pendulum trace.

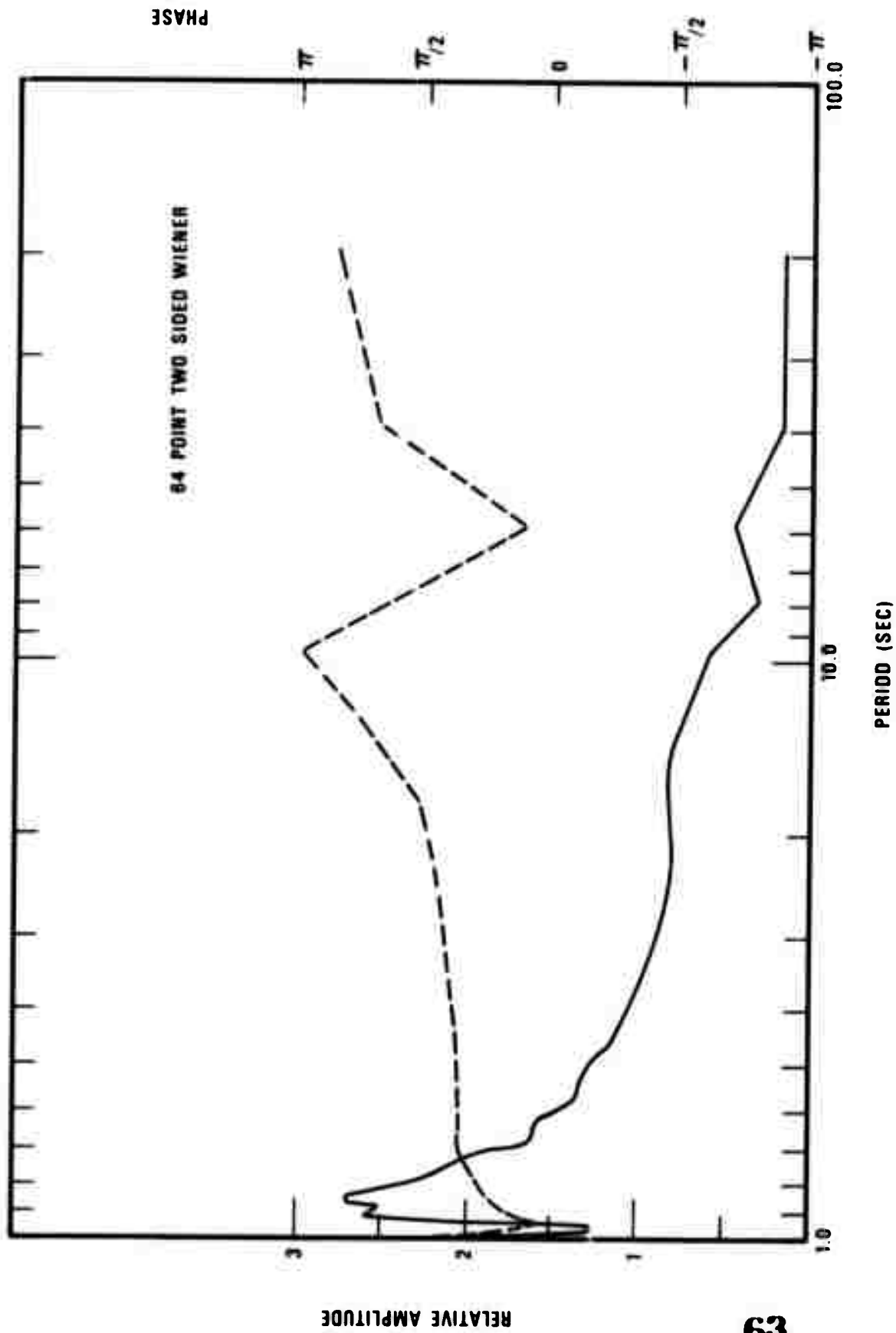


Figure 24. Response of 64 pt Wiener filters designed for noise sample 3 peridium trace.

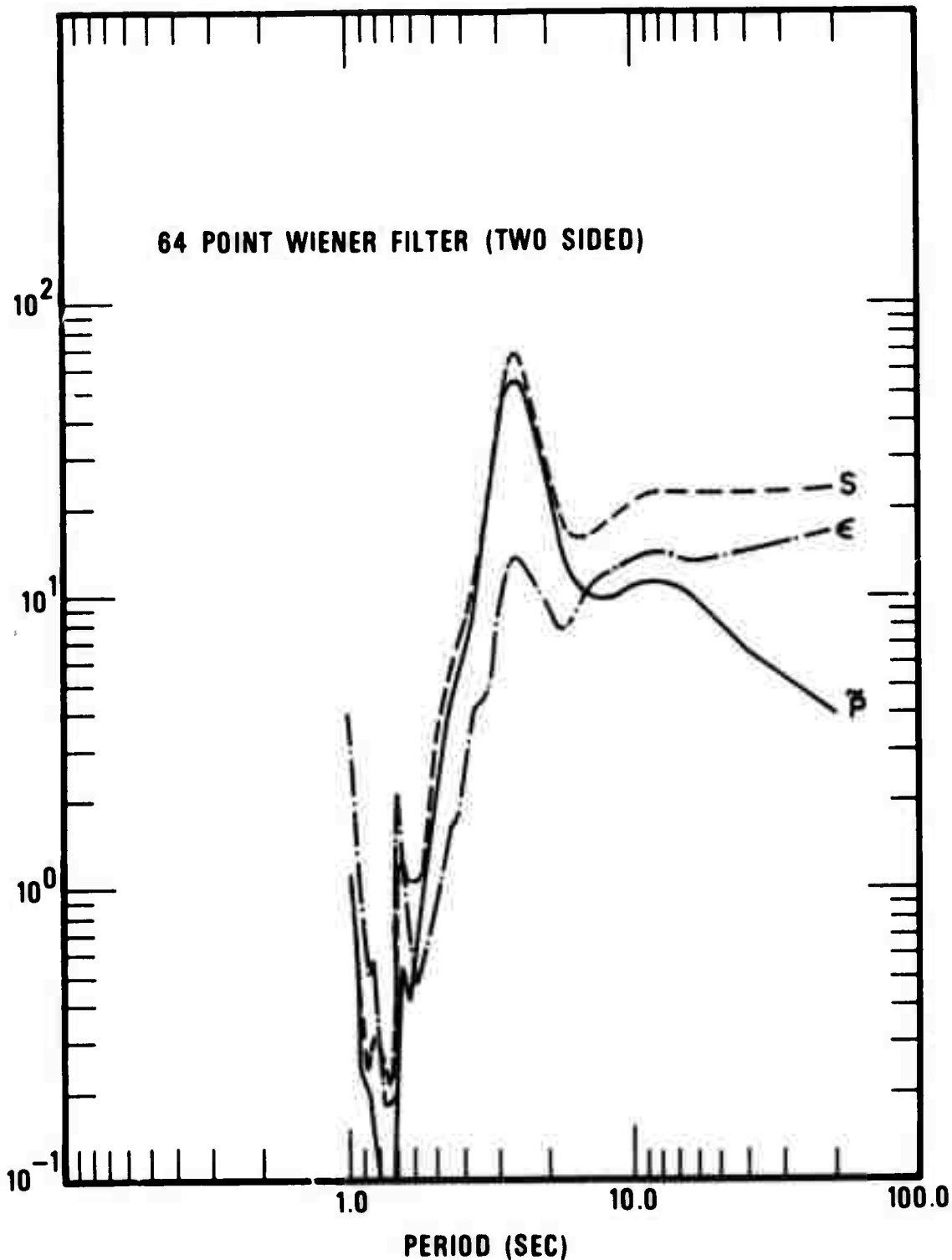


Figure 25. Strain (S), filtered pendulum (\tilde{P}) and error trace power spectra for noise sample 1, after processing by a 64 pt one-sided Wiener filter.

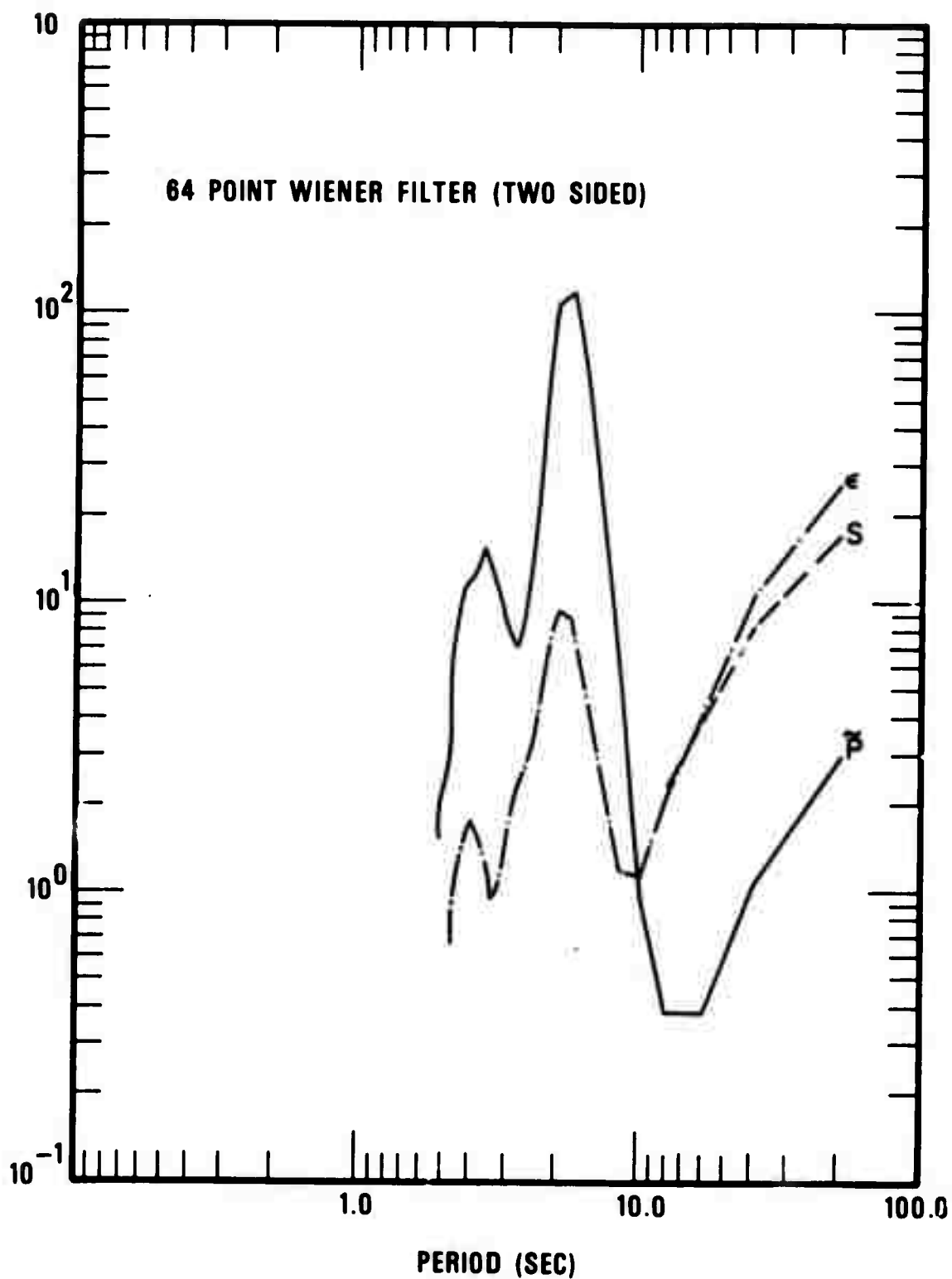


Figure 26. Strain (S), filtered pendulum (\tilde{P}) and error trace power spectra for noise sample 2, after processing by a 64 pt one-sided Wiener filter.

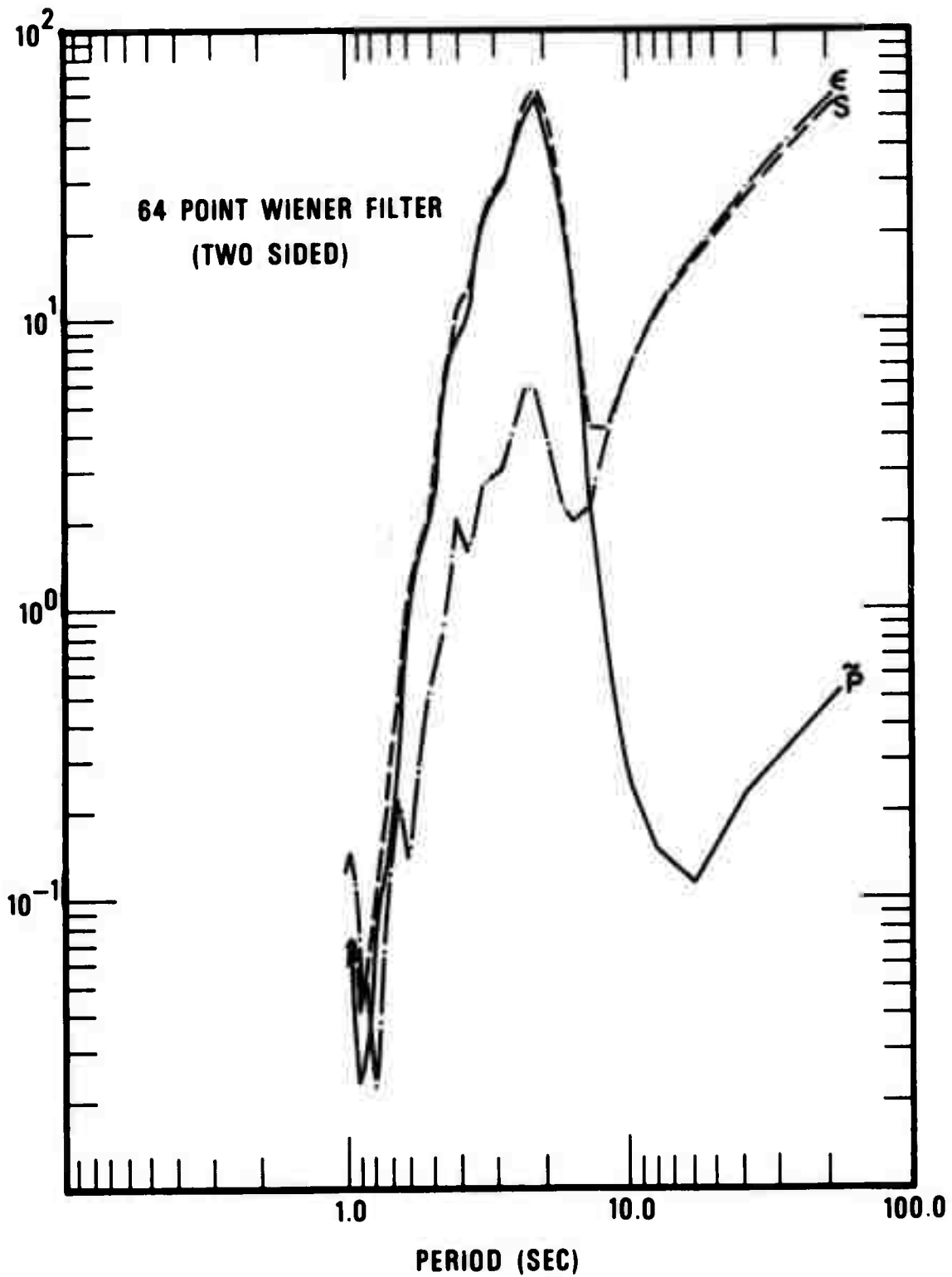


Figure 27. Strain (S), filtered pendulum (\tilde{P}) and error trace power spectra for noise sample 3, after processing by a 64 pt one-sided Wiener filter.

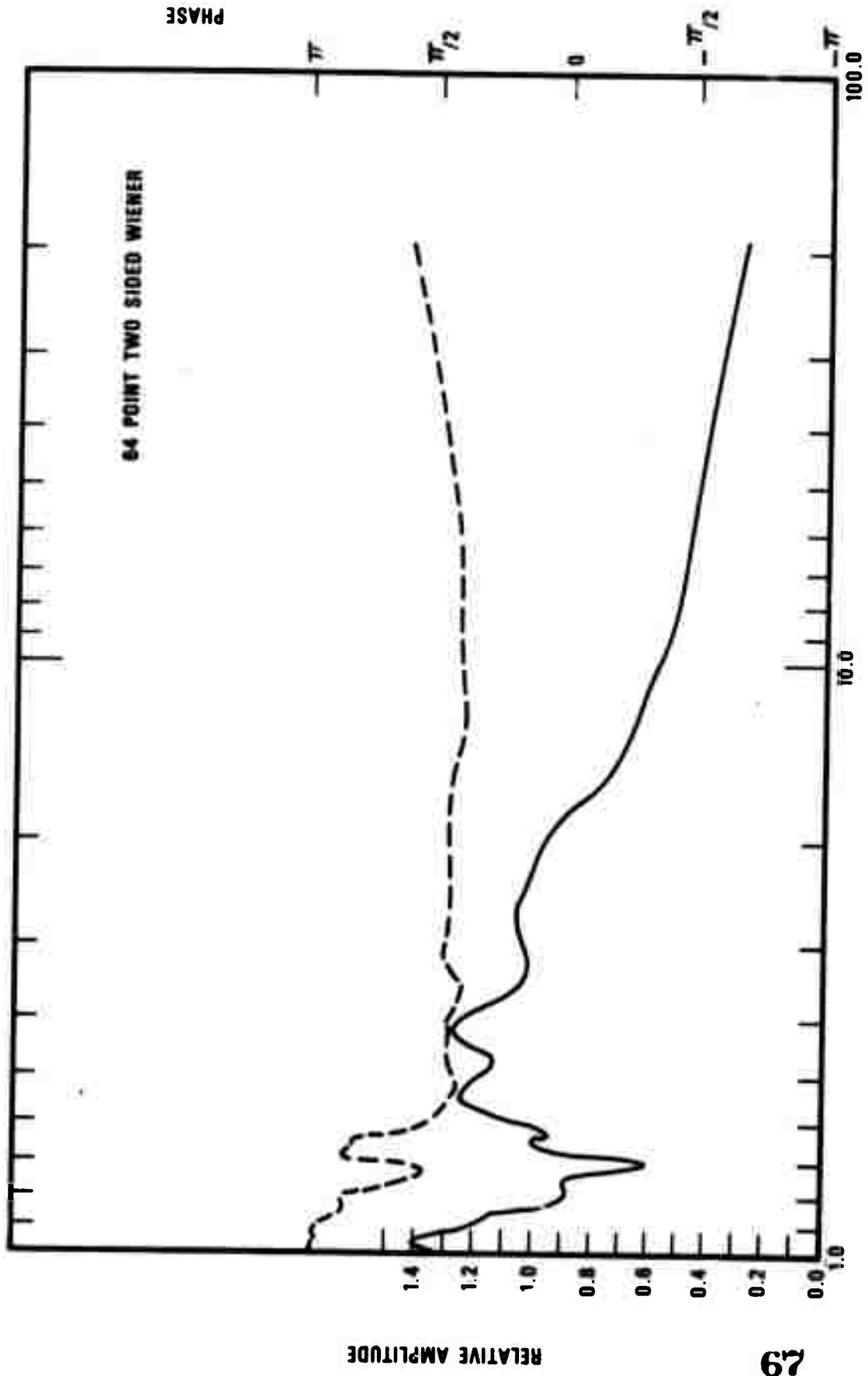


Figure 28. Response of 64 pt two-sided Wiener filter designed for noise sample 1 pendulum trace.

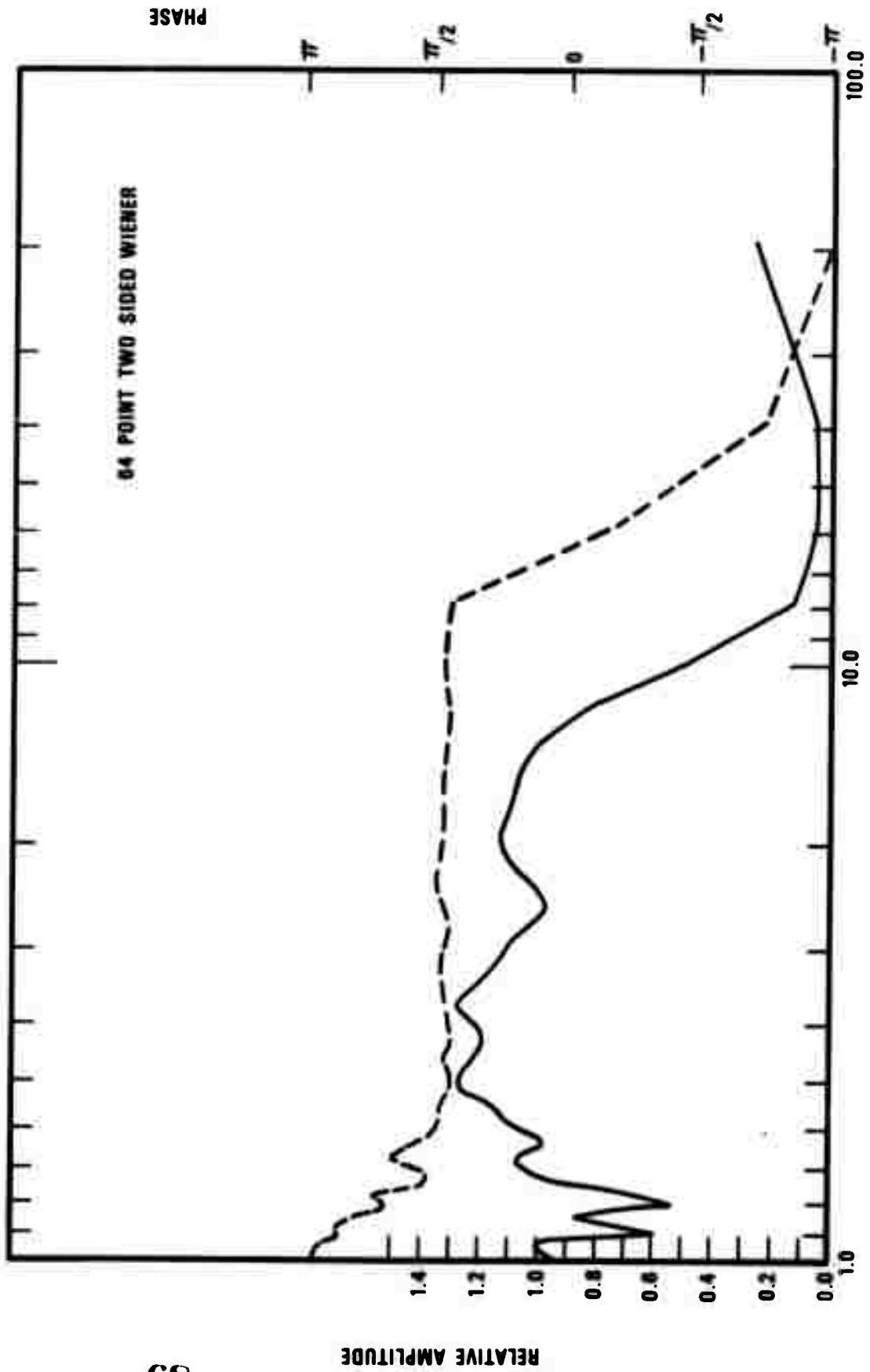


Figure 29. Response of 64 pt two-sided Wiener filter designed for noise sample 2 pendulum trace.

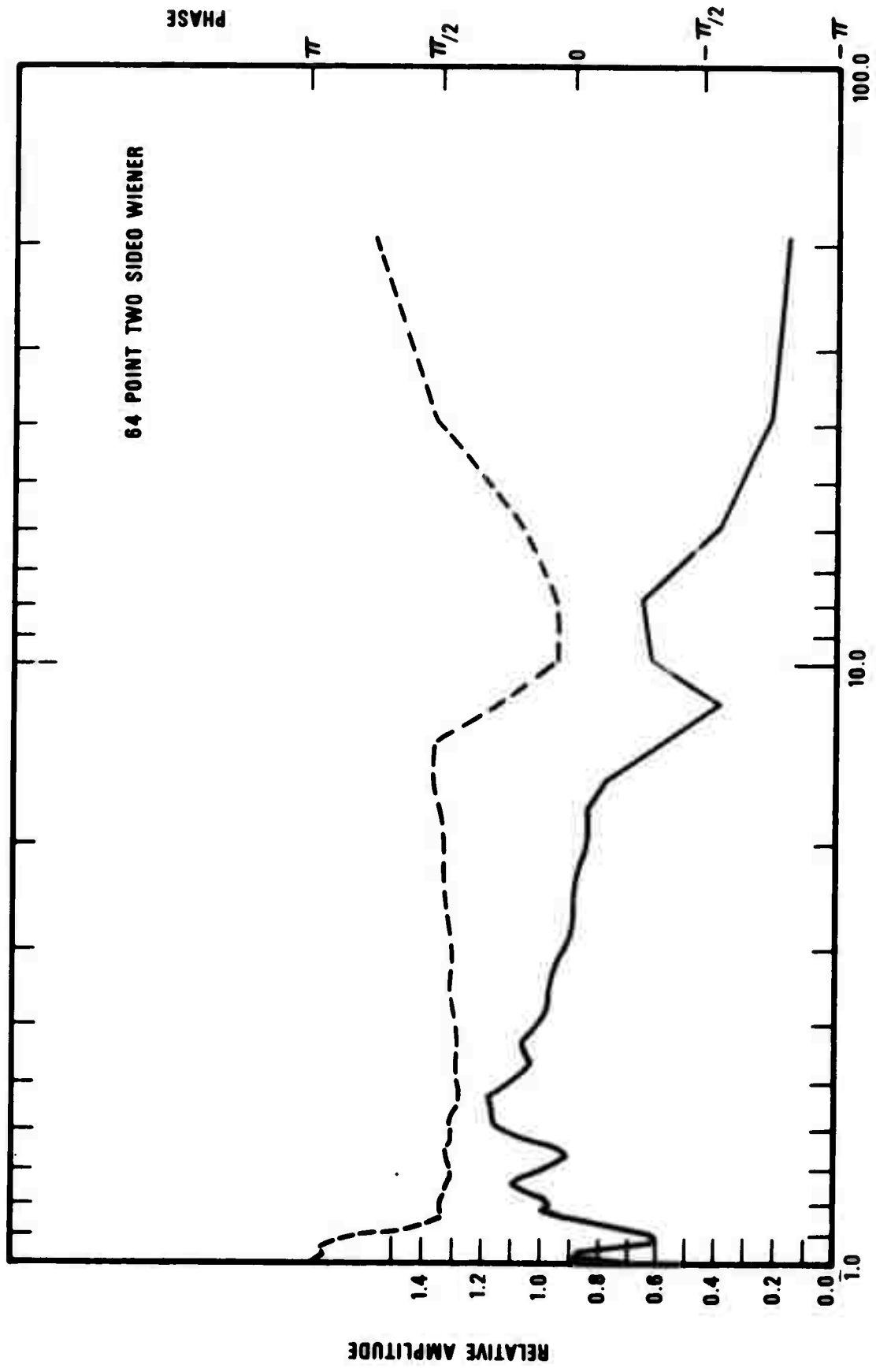


Figure 30. Response of 64 pt two-sided Wiener filter designed for noise sample 3 pendulum trace.

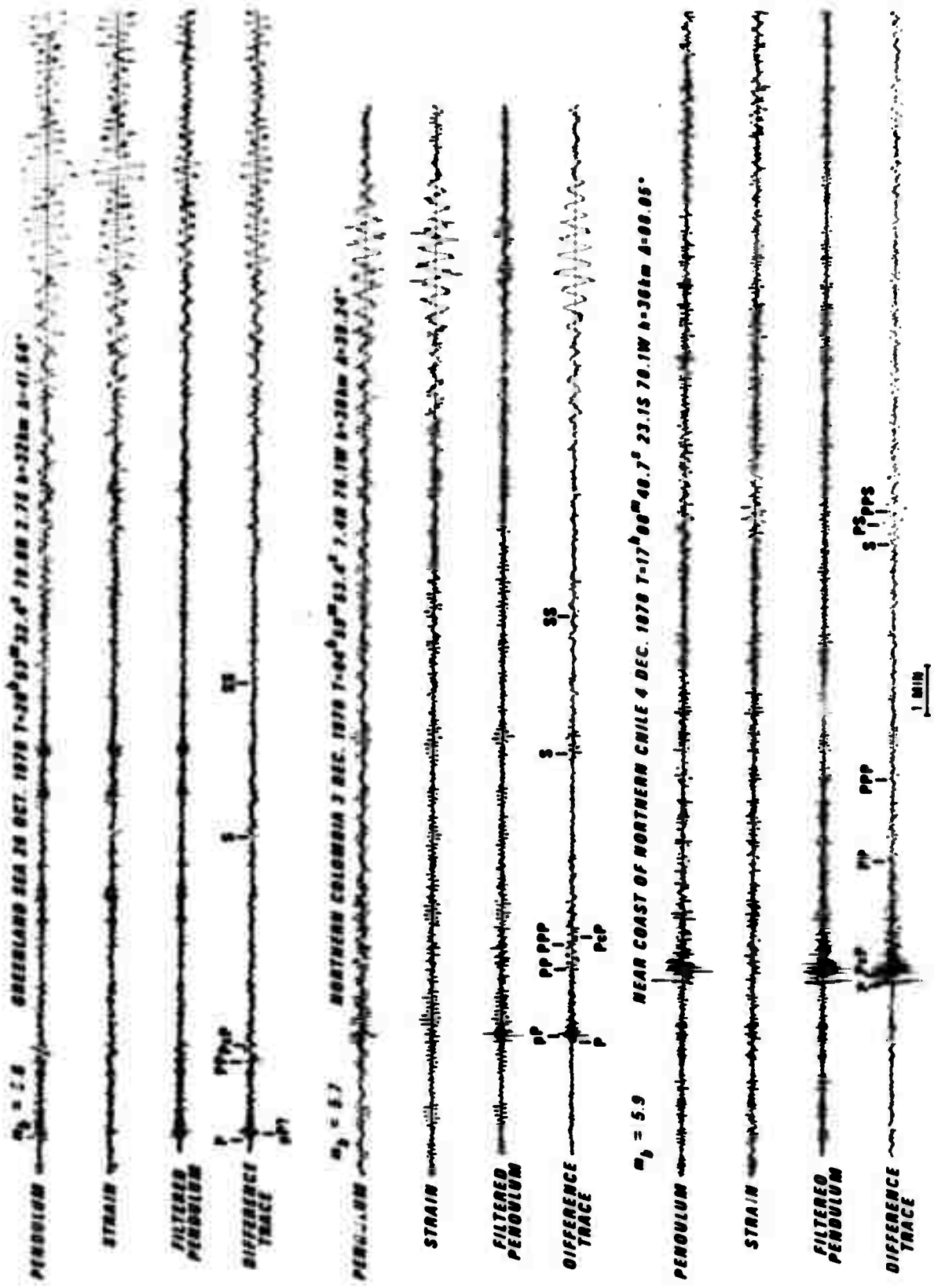


Figure 31. Events processed by a one-sided 64 pt Wiener filter. Amplitude are relative.

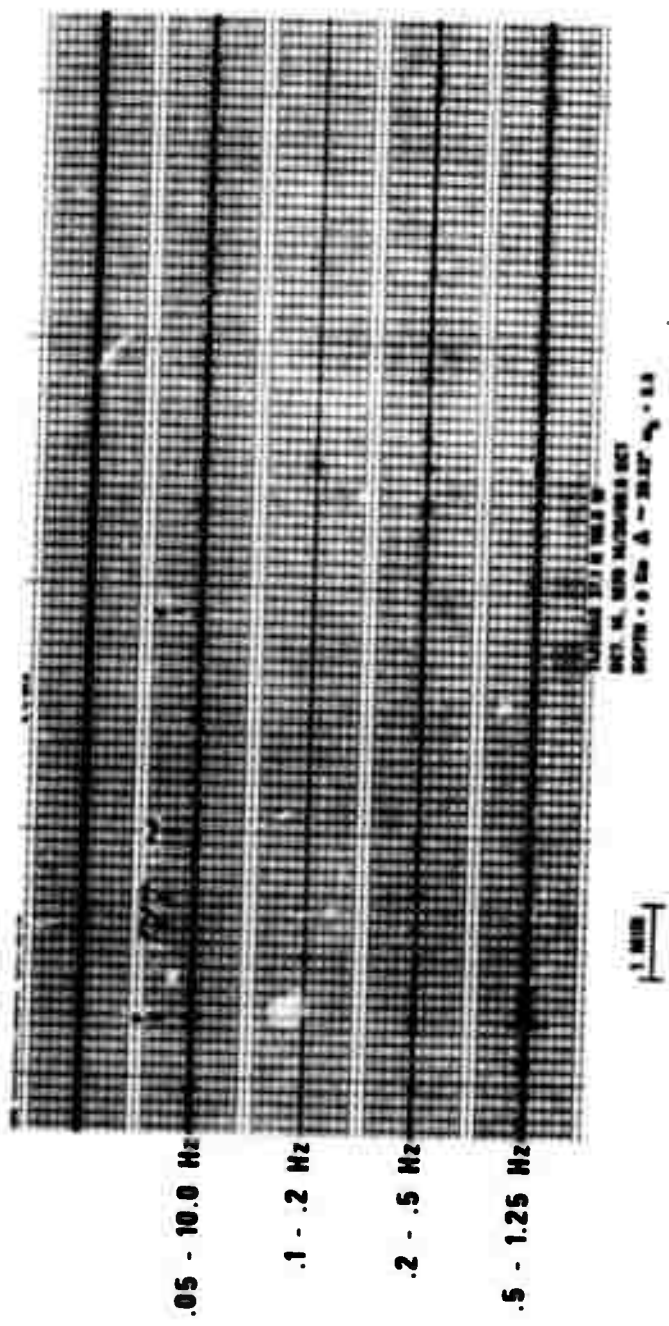


Figure 32. Filtered sum traces for the nuclear explosion TIJERAS. Amplitudes are relative.

Reproduced from best available copy. 6

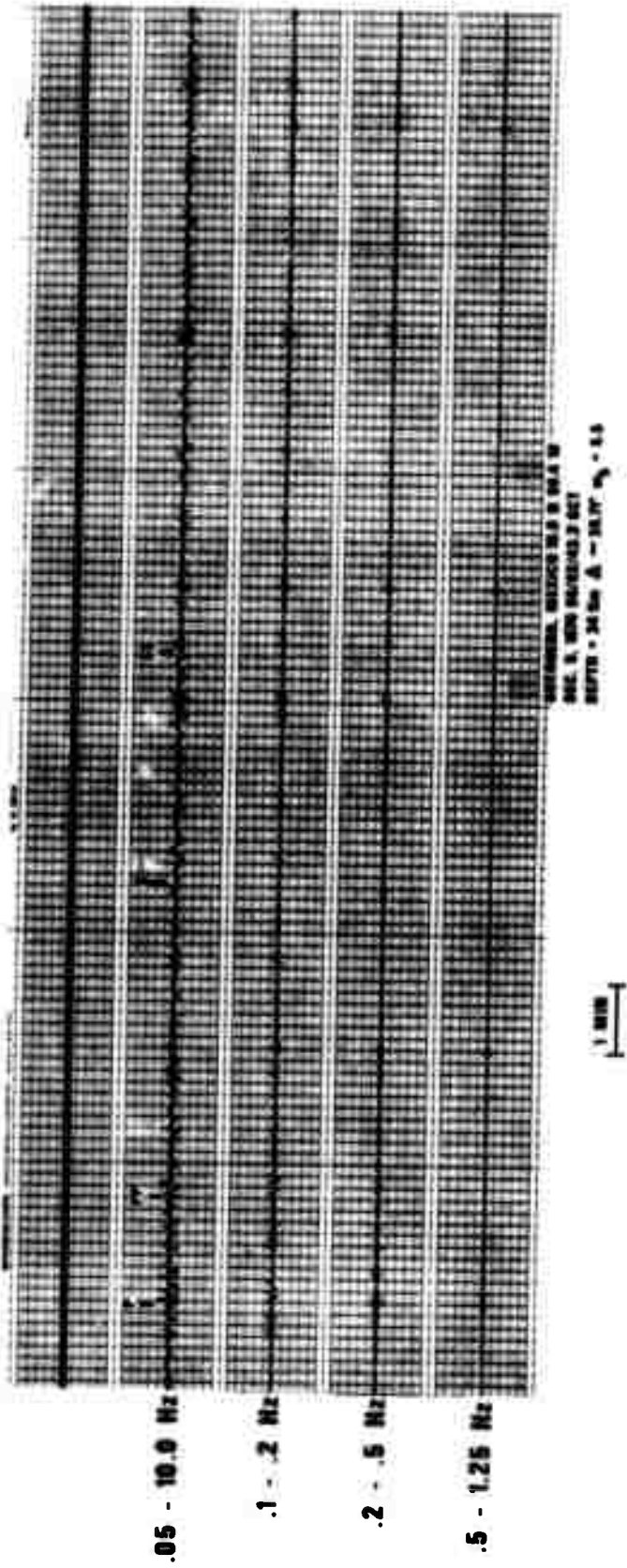


Figure 55. Filtered sum traces for an earthquake from Guerrero, Mexico. Amplitudes are relative.

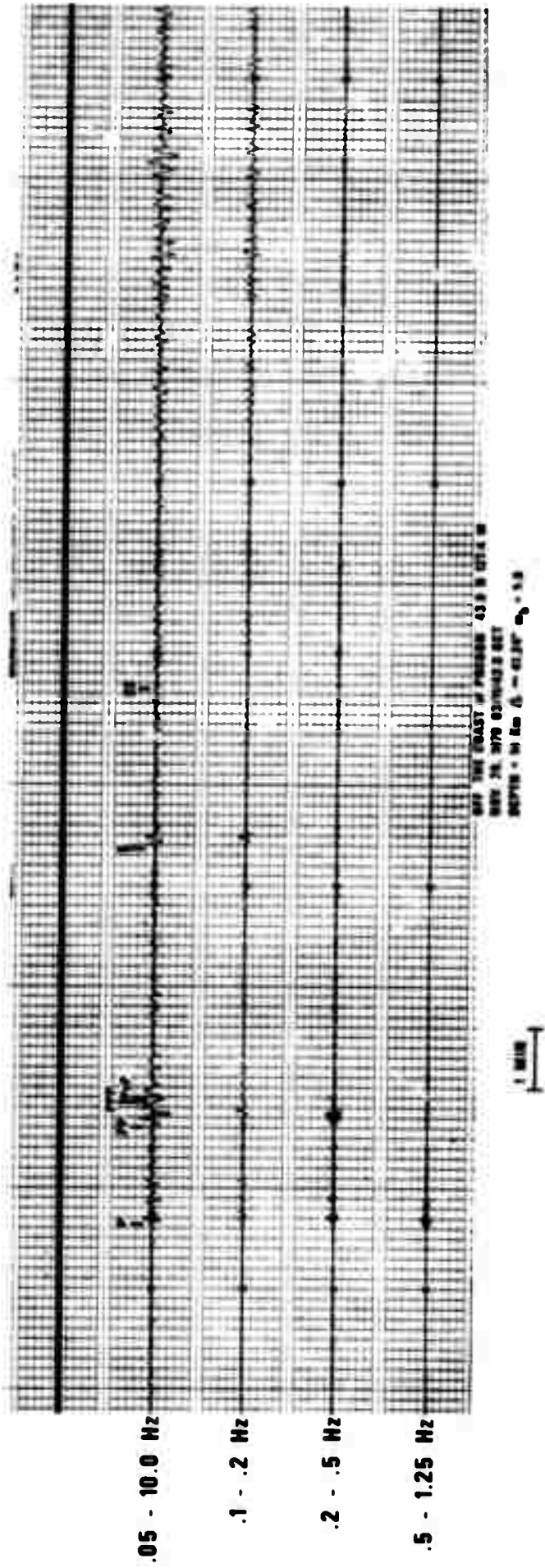


Figure 36. Filtered sum traces for an earthquake off the coast of Oregon. Amplitudes are relative.

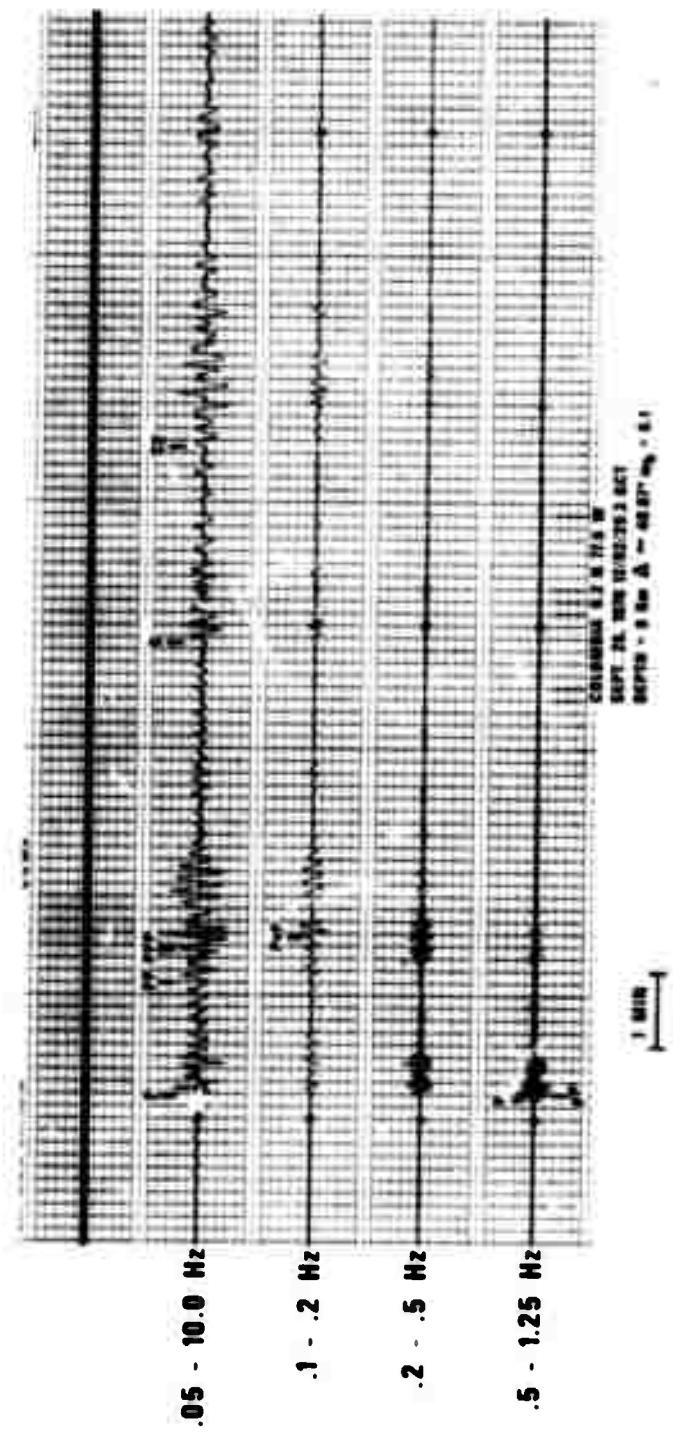


Figure 37. Filtered sum traces for an earthquake from Columbia. Amplitudes are relative.

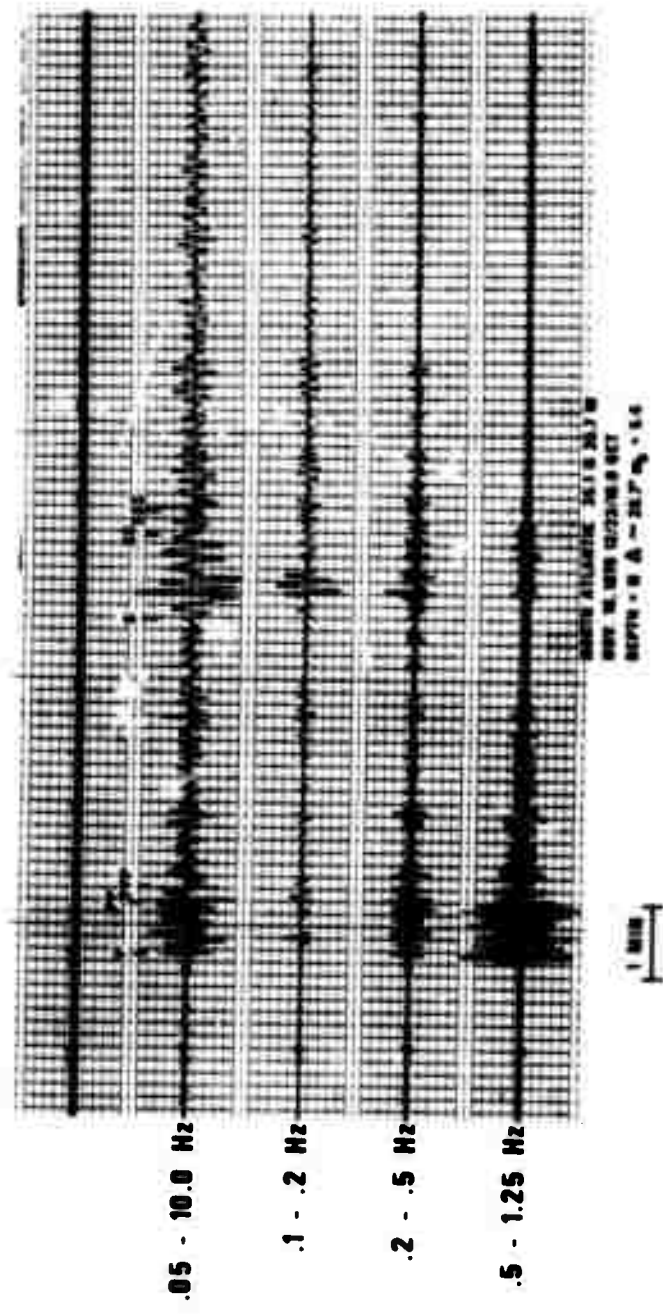


Figure 38. Filtered sum traces for an earthquake from North Atlantic. Amplitudes are relative.

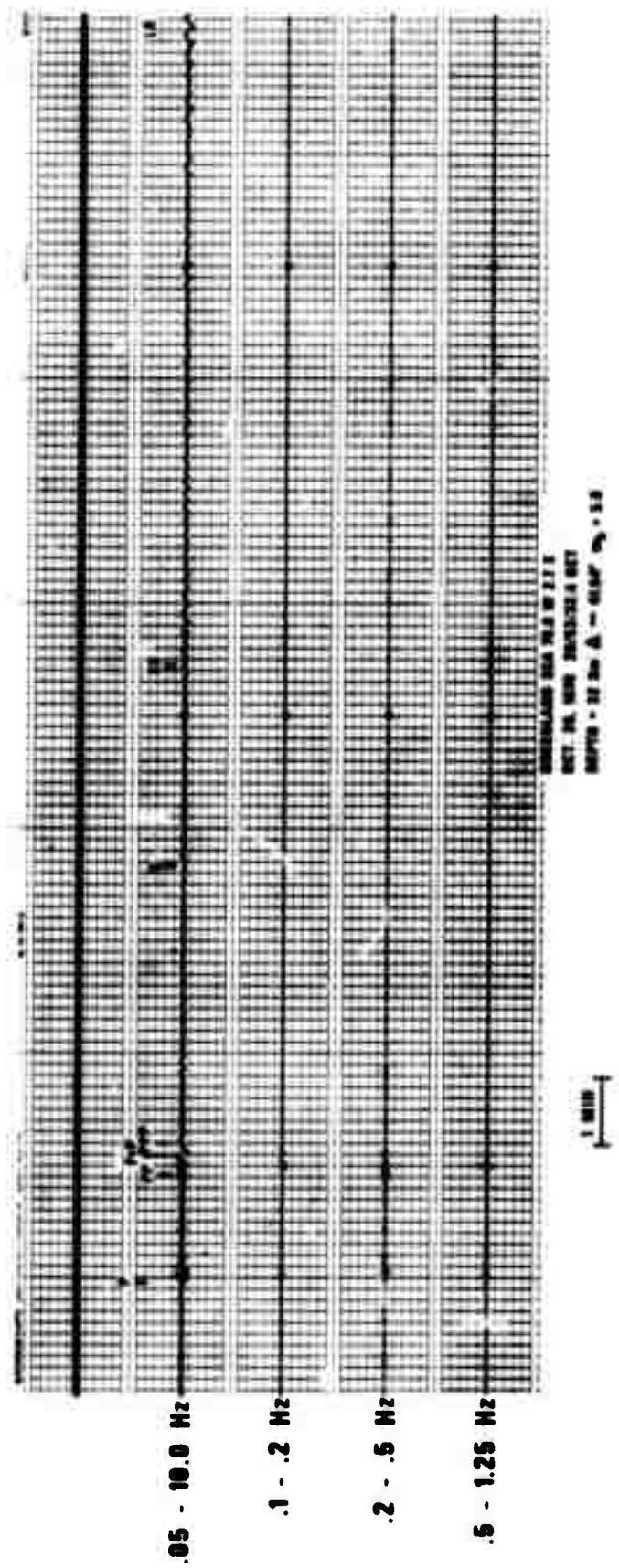


Figure 39. Filtered sum traces for an earthquake from Greenland Sea. Amplitudes are relative.

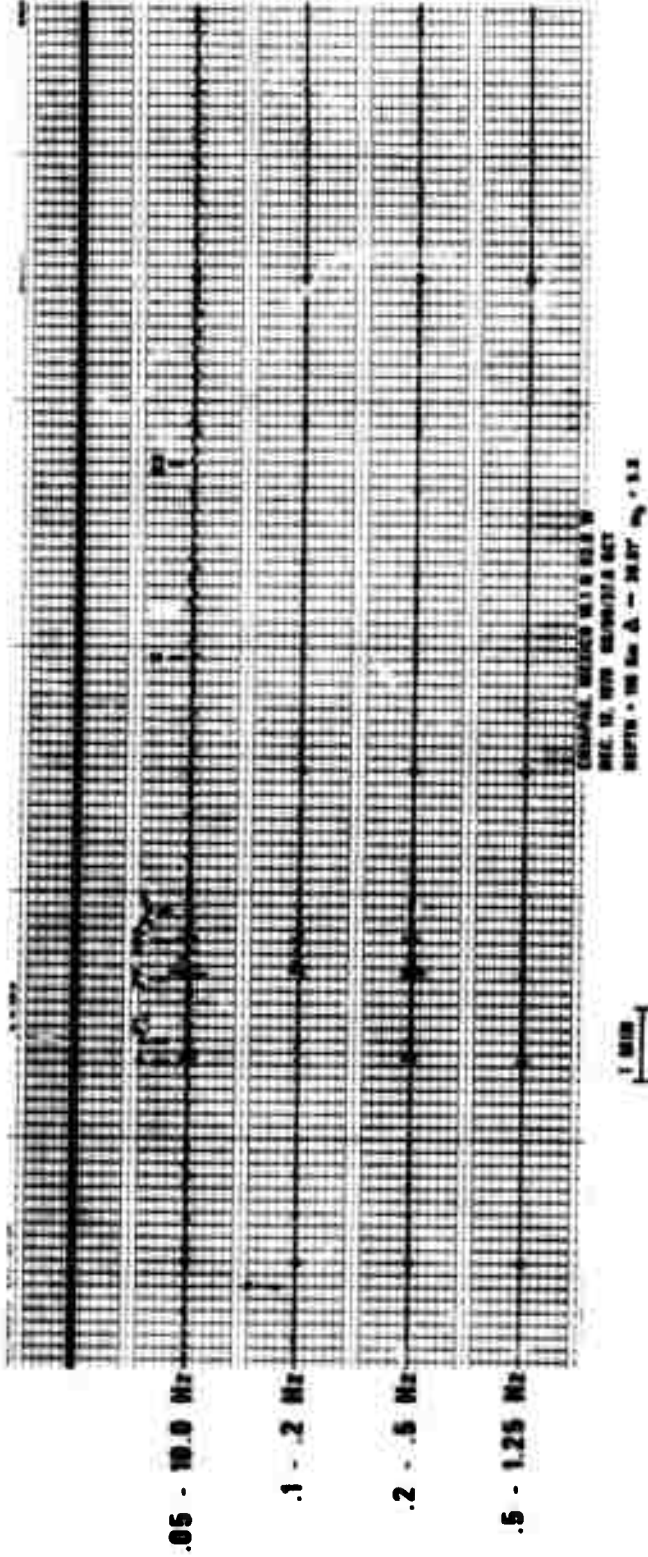


Figure 40. Filtered sum traces for an earthquake from Chiapas Mexico. Amplitudes are relative.

NORTHERN COLOMBIA 3 DEC. 1970 T=4°58'53.6" 7.4N 76.1W h=39km A=39.24°

NR-ME
3 DEC. 1970

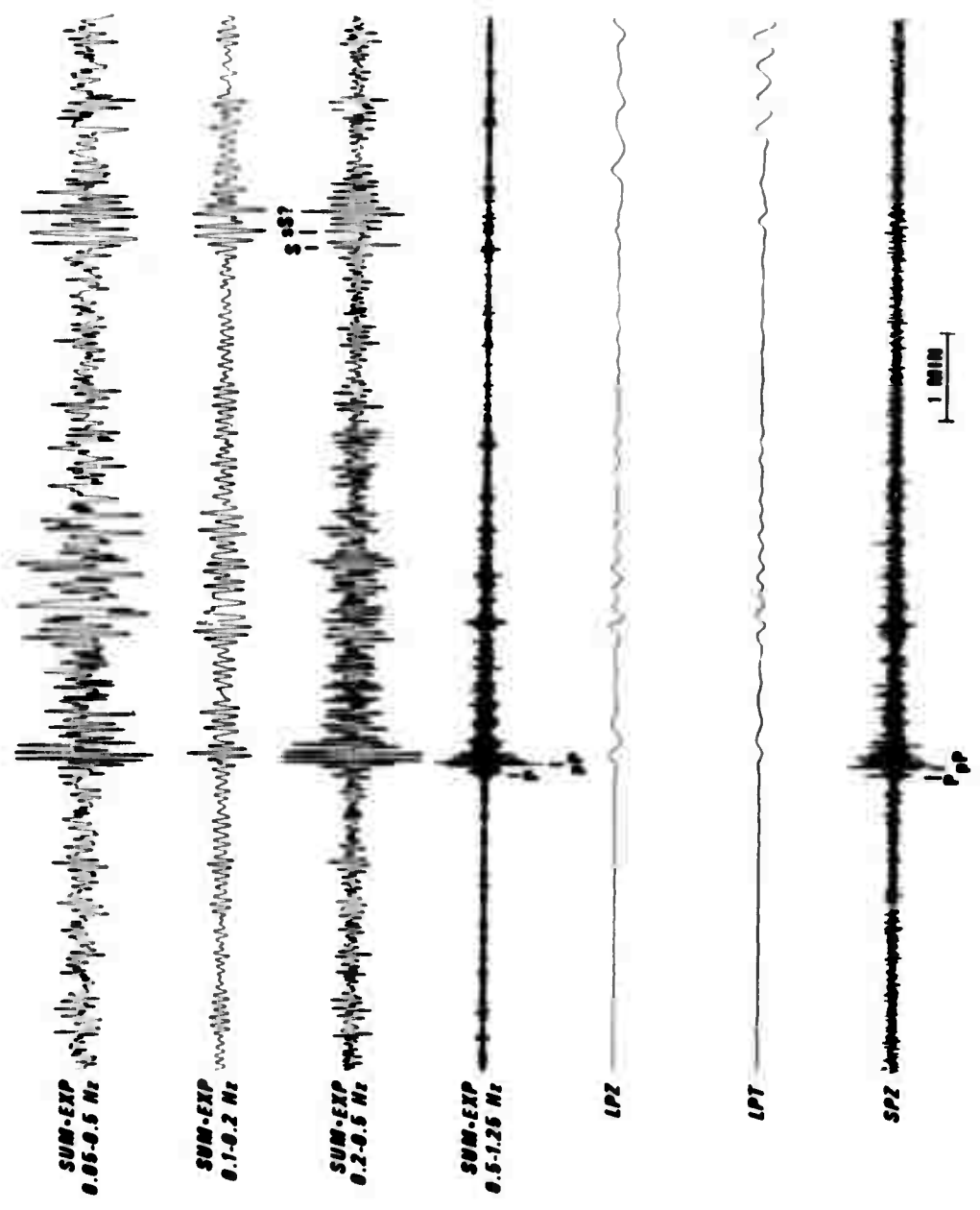


Figure 41. Comparison of depth phases on the filtered intermediate period strain-pendulum sum traces with standard LP and SPZ traces. Amplitudes are relative.